Published in final edited form as:
J Exp Med. 2023 February 06; 220(2): . doi:10.1084/jem.20220906.

SARS-CoV-2 Spike protein suppresses CTL-mediated killing by inhibiting immune synapse assembly

Anna Onnis[1], **Emanuele Andreano**[2], **Chiara Cassioli**[1], **Francesca Finetti**[1], **Chiara Della Bella**[3], **Oskar Staufer**[4], **Elisa Pantano**[2], **Valentina Abbiento**[2], **Giuseppe Marotta**[5], **Mario M D'Elios**[6], **Rino Rappuoli**[2,7], **Cosima T Baldari**[1]

[1]Department of Life Sciences, University of Siena, Siena, Italy

[2]Monoclonal Antibody Discovery (MAD) Lab, Fondazione Toscana Life Sciences, Siena, Italy

[3]Department of Experimental and Clinical Medicine, University of Florence, Florence, Italy

[4]Kennedy Institute of Rheumatology, Nuffield Department of Orthopaedics, Rheumatology and Musculoskeletal Science, University of Oxford, Oxford, UK

[5]Siena University Hospital, Siena, Italy

[6]Department of Molecular and Developmental Medicine, University of Siena, Siena, Italy

[7]Department of Biotechnology, Chemistry and Pharmacy, University of Siena, Siena, Italy

Abstract

CTL-mediated killing of virally infected or malignant cells is orchestrated at the immune synapse (IS). We hypothesized that SARS-CoV-2 may target lytic IS assembly to escape elimination. We show that human $CD8^+$ T cells upregulate the expression of ACE2, the Spike receptor, during differentiation to CTLs. CTL pre-incubation with the Wuhan or Omicron Spike variants inhibits IS assembly and function, as shown by defective synaptic accumulation of TCRs and tyrosine phosphoproteins as well as defective centrosome and lytic granule polarisation to the IS, resulting in impaired target cell killing and cytokine production. These defects were reversed by anti-Spike antibodies interfering with ACE2 binding and reproduced by ACE2 engagement by Angiotensin-II or anti-ACE2 antibodies, but not by the ACE2 product Ang (1-7). IS defects were also observed ex vivo in CTLs from COVID-19 patients. These results highlight a new strategy of immune evasion by SARS-CoV-2 based on the Spike-dependent, ACE2-mediated targeting of the lytic IS to prevent elimination of infected cells.

Correspondence to: Rino Rappuoli; Cosima T Baldari.

Corresponding authors: Cosima T Baldari, Department of Life Sciences, University of Siena, Italy. cosima.baldari@unisi.it; Rino Rappuoli, Fondazione Toscana Life Sciences and University of Siena, Italy. rino.r.rappuoli@gsk.com.
This paper is dedicated to the memory of John L Telford.

Author contributions. AO, EA, CC, FF and CDB did the experiments; AO, CC, FF and CDB analysed the data and prepared the figures; AO, EA, MMdE, RR and CTB wrote the paper; OS, EP, VA and GM provided essential reagents.

Competing interests. RR is an employee of GSK group of companies. EP, VA, EA and RR are listed as inventors of full-length human monoclonal antibodies described in Italian patent applications n. 102020000015754 filed on June 30th 2020, 102020000018955 filed on August 3rd 2020 and 102020000029969 filed on 4th of December 2020, and the international patent system number PCT/IB2021/055755 filed on the 28th of June 2021. All patents were submitted by Fondazione Toscana Life Sciences, Siena, Italy.

Europe PMC Funders Author Manuscripts

Introduction

Severe coronavirus disease 2019 (COVID-19) caused by SARS-CoV-2 infection is associated with immune dysregulation, with defective interferon type I response (Bastard et al., 2020; Zhang et al., 2020), local hyperactivation of innate immune cells and impaired adaptive immune responses, with a prominent role for T cells (Chen and John Wherry, 2020; Kalfaoglu et al., 2021). T cell defects include lymphopenia and dysfunctions that range from excessive activation and exhaustion, to defective activation, to abnormalities in differentiation (Chen and John Wherry, 2020; Kalfaoglu et al., 2021). Interestingly, $CD8^+$ T cells appear preferentially dysregulated in severe COVID-19 compared to $CD4^+$ T cells. A selective decrease in cytotoxic T lymphocytes (CTL) in the upper respiratory tract has been observed in patients with severe disease compared to patients with milder disease (Chua et al., 2020). Additionally, a decrease in cytokine production by $CD8^+$ T cells has been reported in severe COVID-19 (Zheng et al., 2020), while a more robust $CD8^+$ T cell expansion has been associated with milder disease or recovery (Liao et al., 2020; Wen et al., 2020).

As the T cell effectors responsible for the elimination of virally infected cells, CTLs are strategic targets for immune evasion by viral pathogens. A major component of the CTL killing arsenal are lytic granules (LG), lysosome-like organelles enriched in granzymes and perforin that are secreted upon activation (Cassioli and Baldari, 2022). While specificity is dependent on cognate cell recognition by TCR interaction with MHCI-bound peptide antigen (pMHC), selectivity is ensured by the precise delivery of the cytotoxic effectors to the target cell at the immune synapse (IS), a highly specialized signaling and secretory platform that forms at the CTL interface with its target (Douanne and Griffiths, 2021; Dustin and Choudhuri, 2016). TCR engagement triggers a profound rearrangement of receptors, adhesion molecules and co-stimulatory receptors at the target cell contact, which leads to the typical bull's eye architecture of the mature IS. IS assembly is coordinated by the cytoskeleton. An inward actin flow allows for the centripetal movement of TCRs and co-stimulatory receptors to the IS center, eventually forming an F-actin ring that seals a space between the CTL and its target, the synaptic cleft. Additionally, the centrosome and secretory apparatus polarise towards the target cell, with microtubules providing tracks for the transport of the cytotoxic machinery to the IS for delivery into the synaptic cleft (Blumenthal and Burkhardt, 2020; Martin-Cofreces and Sanchez-Madrid, 2018).

Differentiation of $CD8^+$ T cells to CTLs is primed in peripheral lymphoid tissues by DCs that have been activated at the site of infection. Hence the dysregulation of the $CD8^+$ T response by SARS-CoV2 is likely to result, at least in part, from defective priming. However, once differentiated, CTLs migrate to the site of infection, where they can be exposed to high virus concentrations. The finding that the SARS-CoV-2 receptor human angiotensin-converting enzyme 2 (ACE2) (Hoffmann et al., 2020) is expressed in activated T cells and mediates SARS-CoV-2 binding and internalisation (Welch et al., 2022) suggests that, as a result of ACE2 engagement by the Spike protein, T cells may be directly modulated by the virus.

We have hypothesized that, similar to viruses such as HIV-1 (Fackler et al., 2007), SARS-CoV-2 may target IS assembly and function as a means to escape CTL-mediated killing. We provide evidence that Spike suppresses IS assembly in CTLs, leading to impaired cytotoxicity and cytokine production. This effect is dependent on ACE2 interaction and can be reproduced by ACE2 ligands, identifying ligand-bound ACE2 as an inhibitory receptor in CTL activation and a target for immune evasion by SARS-CoV-2.

Results and Discussion

CTLs express the Spike receptor ACE2

While activated T cells have been reported to express the Spike receptor ACE2 (Coppo et al., 2011; Welch et al., 2022), whether this occurs in CTLs has not been investigated. We generated CTLs from $CD8^+$ T cells immunopurified by negative selection from buffy coats from healthy donors and activated using beads coated with anti-CD3 and anti-CD28 mAbs in the presence of IL-2 (Fig.S1A). Under these conditions $CD8^+$ T cells differentiate to functional CTLs by day 5, as assessed by granzyme B (GzmB) expression and cytotoxicity (Fig.S1B,C). Quantitative real-time RT-PCR and immunoblot analyses showed that ACE2 was undetectable or barely detectable in freshly purified $CD8^+$ T cells but was strongly upregulated in CTLs (Fig.1A,B). Consistent with ACE2 expression, Spike was found to bind to CTLs but not freshly purified $CD8^+$ T cells, as assessed by imaging CTLs incubated with Wuhan Spike (Spike-W) and labelled with an anti-Spike mAb (Fig.1C). This was confirmed by imaging CTLs incubated with fluorescently labelled pseudoviral particles (Minimal Virions, MiniVs) assembled in vitro using small unilamellar vesicles with a lipid composition adjusted to resemble the virion lipid membrane and Spike-W ectodomains (~18-40 copies Spike/particle) (Staufer et al, 2022) (Fig.1D).

Spike suppresses IS formation and CTL-mediated cytotoxicity

To test the hypothesis that Spike binding to ACE2 modulates CTL function by targeting the IS, CTLs were pre-treated for 30 min with different concentrations of Spike-W at 20°C to allow for binding but not internalization, and subsequently mixed with Raji B cells pulsed with a mix of the Staphylococcal enterotoxins A, B and E to broadly cover the TCR Vβ repertoire. This is the experimental setting typically used to image IS assembly when using polyclonal human T cells. The experiment was carried out in the absence of serum to rule out potential effects of circulating angiotensins (Ang).

The assembly of functional immune synapses was assessed by measuring the accumulation of tyrosine phosphoproteins and TCR/CD3 complexes at the T cell interface with the APC 15 min following contact with target cells, a time point when the IS has acquired its characteristic architecture. Spike was found to suppress the formation of signaling-competent immune synapses by CTLs in a dose-dependent fashion, as shown by the decreased frequency of conjugates displaying PTyr staining at the IS and the impairment in the synaptic accumulation of tyrosine phosphoproteins (Fig.1E,F; videos 1-3; Fig.S1D,E). Spike also suppressed TCR/CD3 accumulation at the IS (Fig.1E,G; videos 1-3), accounting for the downstream signaling defect. Similar results were obtained when CTLs were pre-treated with MiniVs (Fig.1H,I).

TCR signaling starts immediately upon T cell contact with a cognate APC and is sustained throughout the process of IS maturation. To understand whether Spike interferes with TCR signaling at an earlier stage of IS maturation we compared the outcome of CTL pretreatment with Spike-W on IS assembly in 5-min (nascent IS) versus 15-min (mature IS) conjugates. The defects in phosphotyrosine signaling and TCR/CD3 accumulation at the IS were clearly detectable in 5-min conjugates (Fig.2A,B), indicating that Spike-W impairs TCR signaling at an early step in IS formation. Consistent with this finding, the early synaptic accumulation of active ZAP-70, the protein tyrosine kinase responsible for coupling the TCR to the downstream tyrosine phosphorylation cascade (Au-Yeung et al., 2018), was compromised in Spike-W pre-treated CTLs (Fig.2C). The phosphotyrosine signaling defects were confirmed by flow cytometric analysis (Fig.2D and S1F). Of note, these defects were caused by interference of Spike with TCR signaling and not by steric hindrance at the synaptic contact, as shown by the impairment in TCR-dependent Erk activation in Spike-W pre-treated CTLs activated by TCR cross-linking in the absence of a target cell partner (Fig.2E).

Centrosome repositioning to the IS is essential for the polarized delivery of the cytotoxic effectors of CTLs to the target cell (Douanne and Griffiths, 2021). Co-staining with anti-pericentrin and anti-GzmB Abs showed that centrosome polarization towards the IS was impaired in Spike-W- or MiniV-pre-treated CTLs, as assessed by measuring the distance of the centrosome from the IS center (Fig.3A-C; videos 4-6; Fig.S1D). Additionally, LG convergence towards the centrosome, which is required for efficient degranulation (Daniele et al., 2011; Mentlik et al., 2010), was impaired under these conditions (Fig.3A,D; videos 4-6; Fig.S1D).

The impact of Spike on CTL degranulation was initially tested by measuring the exposure at the plasma membrane of the LG marker LAMP1, which occurs following LG fusion with the plasma membrane. Spike-W pretreatment did not affect the ability of CTLs to degranulate in the presence of SAg-pulsed Raji cells, as assessed on conjugates incubated with fluorescently labelled anti-LAMP1 mAb and analyzed by flow cytometry under non-permeabilizing conditions (Fig.3E). The very low TCR activation threshold for Ca^{2+} mobilization (Irvine et al., 2022), which is essential for CTL degranulation, could account for the the lack of effect of Spike despite the overall impairement in TCR signaling. However, LAMP1 staining was distributed over the entire plasma membrane in SAg-specific conjugates formed using Spike-W-pre-treated CTLs, as opposed to the respective control conjugates, where LAMP1 staining was selectively concentrated at the IS (Fig.3F). No LAMP1 staining was detectable in the absence of SAg (Fig.3F). Hence, Spike pretreatment results in the failure of CTLs to undergo polarized degranulation.

We previously reported that polarized degranulation by CTLs is essential for target cell killing (Kabanova et al., 2016), suggesting that Spike may suppress CTL-mediated cytotoxicity. To address this possibility we carried out fluorimetry-based cytotoxicity assays by incubating Spike-W-pretreated CTLs with SAg-pulsed Raji cells loaded with calcein AM, a cell-permeant dye that becomes fluorescent following hydrolyzation by intracellular esterases and is released by dying cells. Consistent with the defect in LG release at the IS, a time course analysis of fluorescent calcein release by target cells showed that Spike-W suppressed the ability of CTLs to kill target cells at all effector:target cell ratios

tested (Fig.3G) and in a dose-dependent manner (Fig.S1G). Similar results were obtained in an antigen-specific system using as CTLs melanoma-specific CTLs generated from melanoma patients, and as target cells the HLA-matched melanoma cell line A375. For these experiments CTLs were pre-treated with Spike-W or MiniVs, and target cell killing was measured 18 h later by flow cytometry after staining with propidum iodide (Fig.3H,I).

To further confirm the inhibitory effect of Spike on CTL-mediated killing we generated an A375 cell transfectant overexpressing Spike-W and an empty vector control transfectant, and tested their ability to affect CTL function. Spike-overexpressing melanoma cells recapitulated the suppressive effects of Spike pretreatment on CTL cytotoxicity (Fig.3J). Hence Spike-W prevents CTLs from forming functional immune synapses, which results in impaired LG polarization to and release at the IS, thereby compromising their killing potential.

To understand whether Spike impairs CTL function beyond cytotoxicity we assessed their ability to produce cytokines, using IFNγ as a readout. IFNγ quantification in the supernatants of melanoma-specific CTLs activated by autologous B cells pulsed with the melanoma antigen MAGE A3 36 h after conjugate formation showed a reduction in IFNγ production by CTLs pretreated with soluble Spike (Fig.S1H, S2A) or MiniVs (Fig.S2B). Similar results were obtained when melanoma-specific CTLs were mixed with Spike-overexpressing A375 cells (Fig.S2C), indicating that Spike elicits long-lasting inhibitory effects on CTLs.

The inhibitory effects of Spike on IS formation are mediated by ACE2 and can be detected in acutely infected SARS-CoV-2 patients

To achieve insights into the mechanism underlying the suppressive activity of Spike on CTL IS assembly and function, we extended the analysis to the Spike variants Omicron BA.1 and BA.2. These variants recapitulated the effects of Spike-W on IS assembly, as assessed by measuring the synaptic accumulation of tyrosine phosphoproteins and TCR/CD3 complexes (Fig.4A,B), as well as centrosome polarization toward the IS (Fig.4C). Since the mutations carried by the Omicron Spike variants do not compromise ACE2 binding (Wrapp et al., 2020; Yin et al., 2022), this result suggests that the effects of Spike on CTLs are mediated by ACE2. Consistent with this notion, pre-treatment of CTLs with Spike-W or Spike Omicron BA.1 in the presence of specific neutralizing mAbs that prevent Spike binding to ACE2 (Andreano et al., 2021a; Andreano et al., 2021b; Torres et al., 2022) reverted the suppressive effects of the Spike variants on IS assembly by CTLs (Fig.4A-D).

To further address the role of ACE2 in Spike-mediated CTL suppression we investigated the outcome of Spike treatment in freshly purified, quiescent $CD8^+$ T cells, which do not express ACE2 (Fig.1A). Spike did not affect IS assembly in these cells (Fig.S2D-F). However, ACE2 overexpression made quiescent $CD8^+$ T cells responsive to Spike (Fig.4E,D). Hence the inhibitory effects of Spike on IS formation are specifically mediated by ACE2.

To validate these results in the context of SARS-CoV-2 infection we assessed the ability of CTLs naturally exposed to Spike in acutely infected patients to form functional immune

synapses. Mononuclear cells from broncoalveaolar lavage (BAL) and matched peripheral blook lymphocytes (PBL) from three acutely infected patients, and control PBLs from healthy donors, were mixed with SAg-pulsed Raji cells and used to assess their ability to assemble functional immune synapses, as assessed by imaging tyrosine phosphoprotein accumulation at at the APC contact. CTLs were discriminated by the presence of LGs, labelled with anti-GzmB mAb. BALs, but not PBLs, from these patients were found to display severe defects in IS signaling in the absence of exogenously added Spike that recapitulated those observed in healthy, Spike-treated CTLs (Fig.4F). Although other factors may contribute to this phenotype, these data strongly suggest that *in vivo* CTL exposure to Spike in the respiratory tract during acute infection compromises their ability to form functional immune synapses.

ACE2 engagement impairs CTL IS formation and cytotoxicity

ACE2 is a type I transmembrane zinc metalloprotease that plays a key role in the renin-angiotensin system (RAS). The extracellular carboxypeptidase domain of ACE2 catalyses the conversion of Angiotensin (Ang)-I to Ang (1-9), and Ang-II and Ang (1-9) to the bioactive peptide Ang (1-7) which activates the receptor MAS1 on target cells (Samavati and Uhal, 2020). However, ACE2 also acts as a receptor that modulates intracellular processes in a peptidase-independent manner through distinct contributions of its extracellular, transmembrane and intracellular domains, including integrin transactivation, regulation of aminoacid transporters and endocytosis-dependent infection by SARS-CoV-2 (Danilczyk et al., 2006; Hoffmann et al., 2020; Inoue et al., 2007; Simons et al., 2021). To address how ACE2 mediates the suppressive effects of Spike on IS formation we first investigated the localization of ACE2 in SAg-specific conjugates using $CD8^+$ T cells transfected with an ACE2-GFP encoding construct or control GFP-encoding vector. ACE2 was found to accumulate at the IS in the absence of Spike (Fig.5A). Interestingly, ACE2 recruitment to the IS was impaired in the presence of Spike (Fig.5A), suggesting that ACE2 ligands may modulate IS assembly by preventing its correct localization.

We next assessed the outcome of ACE2 engagement on IS assembly in CTLs, using as ligand an anti-ACE2 polyclonal Ab raised against the extracellular domain that blocks SARS-CoV-2 entry in target cells by competing with Spike for ACE2 binding (Hoffmann et al., 2020). CTL pretreatment with the anti-ACE2 Ab recapitulated the suppressive effects of Spike on IS assembly, including the synaptic accumulation of tyrosine phosphoproteins and TCR/CD3 complexes (Fig.5B,C), centrosome polarization toward the IS (Fig.5D) and LG convergence toward the centrosome (Fig.5E). Consistently, CTL-mediated killing (Fig.5F,G) and IFNγ production (Fig.S3A) were suppressed under these conditions. Similar to Spike, the anti-ACE2 Ab suppressed the formation of signaling-competent immune synapses in CTLs at an early maturation step, as assessed by analyzing immune synapses formed in 5-min versus 15-min CTL-target cell conjugates (Fig.S3B-D). No effect on IS assembly was observed when freshly purified $CD8^+$ T, which do not express ACE2 (Fig.1A), were pre-treated with the anti-ACE2 Ab (Fig.S3E-G). Of note, while AngII suppressed the assembly of functional immune synapses in CTLs, similar to the anti-ACE2 Ab, no effect was observed when cells were treated with Ang (1-7) (Fig.5B-E), ruling out the catalytic activity of ACE2 in this function as well as indirect effects mediated by the Ang (1-7) receptor

MAS1. Of note, while MAS1 was expressed in $CD8^+$ T cell, its expression decreased during their differentiation to CTLs (Fig.S3H). Taken together, these results support the notion that, following ligand binding, ACE2 delivers inhibitory signals to suppress IS assembly.

Collectively, our results provide novel insight into the mechanisms of immune evasion by SARS-CoV-2, involving the Spike-ACE2 axis, as a means for infected cells to avoid killing. We believe that the effects that we observed *in vitro* can be related to the physiological setting of SARS-CoV-2 infection, as strongly supported by the IS defects in CTLs from acutely infected patients. Of note, it has been calculated that during infection *in vivo* individuals carry up to 10^{11} virions/ml in sputum (Bar-On et al., 2020) or 10^{11} virions in the lungs (Sender et al., 2021), which translates into ~4 μg of Spike protein, an amount that is in the range of the one we used in vitro. Given that the virus multiplies at the epithelial level, we believe that the local concentration of the Spike may easily exceed the levels used in our *in vitro* experiments. In addition, while soluble Spike was able to suppress CTL IS assembly and cytotoxicity, each virus displays ~60 copies of the Spike trimer on its surface, which is likely to amplify signaling through receptor clustering. In support of this notion MiniVs, which carry ~18-40 copies of trimeric Spike (Staufer et al., 2022), suppressed IS assembly and function of CTLs at a concentration >2-fold lower than soluble trimeric Spike (legend to figure 1H).

The mechanism underlying the inhibitory effects of Spike on IS assembly remains to be elucidated. Our data show that SARS-CoV-2 Spike protein binding to ACE2 interferes with the assembly of a functional IS in CTLs by inhibiting the process at an early step, concomitant with ACE2 exclusion from the IS. Potential targets of the ACE2-Spike axis are integrins such as LFA-1, which is essential for the generation of well-structured immune synapses characterised by the tight accumulation of TCR/CD3 complexes at the center of the contact area with the APC (Cassioli et al., 2021a). ACE2 has been reported to constitutively interact with β1 and α5 integrins, promoting cell adhesion and modulating downstream signaling (Clarke et al., 2012; Lin et al., 2004). Whether ACE2 binds to and modulates signaling by T cell integrins is as yet an open question. The finding that ACE2 is recruited to the IS and fails to do so when engaged by ligand suggests the intriguing possibility that, in the absence of ligand, ACE2 may contribute to IS assembly by promoting integrin-dependent adhesion.

It is noteworthy that, close to the ACE2 binding site, Spike displays a conserved RGD sequence, the consensus integrin-binding motif (Sigrist et al., 2013). Experimental evidence supports the notion that β1 and αv integrins may act as alternative Spike receptors or co-receptors together with ACE2 (Norris et al., 2022; Park et al., 2021). Mechanistically, Spike has been shown to modulate β1 integrin signaling in the kidney cell line Vero E6 for productive infection by activating inside-out signaling mediated by Gα13 and adaptor talin (Simons et al., 2021). Additionally, the RGD sequence within the ACE2-binding domain of Spike has been recently identified as an αv-selective integrin agonist in primary human airway epithelial cells, where it triggers cell spreading, formation of focal adhesions and actin reorganisation through the activation of the kinases FAK and Src, and the adaptor paxillin (Norris et al., 2022). However, the fact that integrin activation is a key activating event required for the onset of IS assembly (Springer and Dustin, 2012) and that Spike

suppresses this process, strongly suggests that the inhibitory effects of Spike on the CTL IS are not mediated by integrins. Additionally, our data show that the Spike Omicron BA.2 variant, which carries a non-conservative D to N substitution at position 405 of the RGD integrin binding motif mapping at positions 403-405 (RGN), is as effective as Spike-W and Spike Omicron BA.1 at suppressing IS assembly. Conversely, the ability of mAbs that prevent Spike binding to ACE2, together with the lack of any effect of Spike on IS assembly in freshly purified $CD8^+$ T cells that do not express ACE2 but their acquired susceptibility to Spike following forced ACE2 expression, highlights the key role of ACE2 in the Spike-dependent suppression of IS assembly and CTL-mediated killing.

While the role of ACE2 as an ectoenzyme that participates in the RAS has been extensively characterized, the role of its transmembrane and intracellular domains, that together display 48% identity with collectrin (Zhang et al., 2001), are only beginning to be explored. Both domains have been implicated in SARS-CoV-2 infection through the endocytic uptake of the virus following Spike-mediated binding to the extracellular domain of ACE2 (Hoffmann et al., 2020; Inoue et al., 2007). Additionally, the collectrin homology domain has been shown to act as a chaperone to stabilise transporters of large neutral aminoacids at the surface of intestinal epithelial cells to regulate aminoacid absorption (Camargo et al., 2009; Kowalczuk et al., 2008). The intracellular domain also regulates the TACE/ADAM17-mediated shedding of the extracellular domain to its catalytically active soluble form by interacting with calmodulin (Lambert et al., 2008). Of note, CTLs could become susceptible to SARS-CoV-2 infection as a result of ACE2 expression, and indeed this possibility has been proven in total activated peripheral T cells (Welch et al., 2022), suggesting that CTLs might first be disabled by Spike targeting of the IS and then killed by CTLs newly recruited to the site of infection.

The inhibitory effects of ACE2 ligands, but not of the product of its catalytic activity Ang(1-7), on TCR signaling and IS assembly support the notion that ACE2 limits CTL activation in a peptidase-independent fashion through signals triggered in response to ligand binding. Since anti-ACE2 antibodies have been shown to be effective in limiting SARS-CoV-2 production in cellular and animal models (Chen et al., 2021; Chaouat et al., 2022), our findings raise the possibility that using these antibodies as therapeutics in COVID-19 patients may lead to unwanted immune suppression.

It is noteworthy that a functional RAS has been documented in T cells (Coppo et al., 2011). Among the RAS components, the Ang-II receptor AT1 has been reported to have immunomodulatory effects on T cells, limiting harmful $CD8^+$ T cell responses during blood-stage malaria and promoting a protective $CD4^+$ T cell response in the kidney in the setting of hypertension (Silva-Filho et al., 2016; Silva-Filho et al., 2017; Zhang et al., 2012). This suggests that ACE2 may participate in T cell immunity through both its enzyme-independent and its enzyme-dependent activities.

Other viruses have co-opted the T cell IS as a target to escape immunosurveillance. One of the most striking examples is HIV-1, which exploits the virulence factor Nef to subvert the process of vesicular trafficking required for the coordinated transport of key signaling components to the IS, leading to a nonproductive T cell response against the virus (Fackler

et al., 2007). Importantly, the IS acts a signaling and cell-cell communication platform also for other immune cells, including helper T cells and B cells (Batista et al., 2001; Chemin et al., 2012; Papa and Vinuesa, 2018). The data reported here highlight the intriguing possibility that SARS-CoV-2 may co-opt IS targeting as a wide-ranging immunomodulatory strategy, beyond suppression of CTL function, to evade the adaptive immune response of the host.

Materials and Methods

Cells, plasmids and antibodies

Peripheral blood and BAL samples were obtained after informed consent according to the Declaration of Helsinki. Experiments were performed after approval by the local ethics commitees (Comitato Etico Regione Toscana Area Vasta Sud Est and Area Vasta Centro).

Primary human $CD8^+$ T cells were isolated from buffy coats of healthy donors and purified (>95%) by negative selection using the RosetteSep™ Human $CD8^+$ T Cell Enrichment Cocktail (StemCell Technologies, #15063), according to the manufacturer's instructions. $CD8^+$ T cells were cultured immediately following isolation at 37°C, 5% CO_2, in RPMI-HEPES medium (Merck, #R7388) supplemented with 10% iron-enriched bovine calf serum (BCS; GE Healthcare HyClone, #SH30072.03) and 1% MEM Non-essential amino acids (MEM NEAA) (#11140050) at the density of 1×10^6/ml.

Melanoma-specific $CD8^+$ T cells were derived from the peripheral blood of three melanoma HLA $A02^+$/HLA $A24^+$ patients. Briefly, PBMCs were isolated by Ficoll-Hypaque density gradient centrifugation (Lymphoprep™, Alere Technologies, Oslo, Norway). A portion of them was frozen in DMSO 10% at -80°C for future use as APCs. The remaining part was incubated with CD8 MicroBeads for the MACS® cell separation method (Miltenyi Biotec, Germany, https://www.miltenyibiotec.com/IT-en/products/macs-cell-separation.html). $CD8^+$ T cells purified from donors, according to the manufacturer's protocol, were co-cultured with 1×10^6 irradiated A375 melanoma cells (ATCC, Manass, VA, USA) and 0.5×10^6 irradiated autologus APCs in RPMI 1640 complete medium to obtain $CD8^+$ cell lines specific for A375 melanoma cells. After ten days from of co-culture CTLs were analyzed for their responsiveness to melanoma A375 and MAGE A3 antigens by measuring [^{3}H]-thymidine uptake (D'Elios et al., 1997).

Bronchoalveolar lavage (BAL) samples from severely affected SARS-CoV-2 patients were collected and layered on Ficoll-Hypaque density gradient in order to isolate bronchoalveolar lavage-derived T cells as described (Amedei et al., 2009). Peripheral blood lymphocytes (PBL) were isolated from the same patients as well as from healthy donors by Ficoll-Hypaque density gradient.

The Burkitt Lymphoma derived B cell line Raji was grown at 37°C, 5% CO_2, in RPMI-1640 Medium (Merck, #R8758) supplemented with 7.5% BCS. The melanoma line A375 (ATCC) was grown in DMEM High Glucose (EuroClone, #ECB7501L) supplemented with 10% FCS. To investigate the effects of cell-bound Spike on CTL function, a Spike-overexpressing A375 transfectant was generated with a Spike-W-encoding pcDNA3 construct. Cells were

transfected using the Turbofect transfection reagent (Thermofisher) and tested after 24 h for Spike expression at the plasma membrane by flow cytometry. An empty vector transfectant was generated as negative control.

Plasmids included pcDNA3 (ThermoFischer), pcDNA3-Spike W (Addgene #145032) and pcDNA3-ACE2-GFP (Addgene #154962). The Wuhan Spike protein was generated using a plasmid encoding the SARS-CoV-2 S-2P construct (Wrapp et al., 2020). The Omicron BA.1 Spike protein was generated using the SARS-CoV-2 S HexaPro construct (Addgene ID: 154754) containing the Spike sequence of this variant.

Primary commercial antibodies used in this work for immunofluorescence analysis were from SantaCruz (CD3ζ, clone 6B10.2, #sc-1239), Cell Signaling (P-ZAP-70 Y319/ Syk Y352, #2701S; PTyr, #8954S), Abcam (Pericentrin, #4448), BD Biosciences (Granzyme B, #560211) and BioLegend (APC anti-human CD107a/LAMP1, #328619). Alexa Fluor 488-, 555- and 647-labeled secondary antibodies were from ThermoFisher Scientific (anti-mouse 488, #A11001; anti-mouse 555, #21422; anti-rabbit 555, #A21428; anti-rabbit 647, #A21244).

SARS-CoV-2 Spike protein expression and purification

Plasmids encoding the Wuhan Spike (Spike-W) and Spike Omicron BA.1 and BA.2, were transiently transfected in Expi293F™ cells and ExpiCHO-S cells (Thermo Fisher) respectively. Cells were grown for six days at 37 °C with 8% CO_2 shaking 125 rpm according to the manufacturer's protocol (Thermo Fisher). Cell cultures for Spike-W and Spike Omicron BA.1 and BA.2 were harvested six days after transfection. Collected supernatants were clarified by centrifugation (1,200 × g, 30 min, 4°C) followed by filtration through a 0.45 μm filter. Chromatography purification was conducted at room temperature using ÄKTA go purifier system from GE Healthcare Life Sciences. Filtrated culture supernatants were purified with a 5 ml HisTrap FF Crude column (GE Healthcare Life Sciences) previously equilibrated in Buffer A (20 mM NaH_2PO_4, 500 mM NaCl + 30 mM Imidazol pH 7.4). Spike proteins were eluted from the column with 5 column volumes of 60% Buffer B (20 mM NaH_2PO_4, 500 mM NaCl + 500 mM Imidazol pH 7.4). Eluted fractions were pooled and dialyzed with PBS buffer pH 7.4 using Slide-A-Lyzer™ Dialysis Cassette 10K MWCO (Thermo Scientific) overnight at 4°C. The final Spike protein concentration was determined by measuring the absorbance at 562 nm using Pierce™ BCA Protein Assay Kit (Thermo Scientific). Final proteins were dispensed in aliquots of 0.5 ml each and stored at -80°C prior to use.

Minimal SARS-CoV-2 virions (MiniVs)

Synthetic virions were formed as described previously (Staufer et al., 2022). Briefly, liposomes were produced with a composition of 45 mol% DOPC, 21 mol% DOPE, 3 mol% DOPS, 12 mol% DOPI, 14 mol% cholesterol, 3 mol% SM and 1mol% DGS-NTA(Ni^{2+}) with a diameter of 108 nm ± 23 nm by extrusion in phosphate buffered saline. All lipids were obtained from Avanti Polar Lipids (USA). To image the localization and binding of the synthetic virions by fluorescence microscopy, 1mol% fluorescent NBD-labelled PE lipids where included to the initial lipid mixture used for liposome preparation. To form

synthetic virions, recombinant histidine-tagged SARS-CoV-2 Spike protein (aa16-1213, Thermo Fischer RP-87671) was conjugated to the liposomes to yield a final density of 18-40 Spike proteins per vesicle. Conjugation was performed for at least 20 min at 4°C in the dark. To analyze T cell-target cell synapse formation and cytotoxicity, the synthetic virions solution was diluted to a final particle concentration of 1.2×10^9/mL in culture medium, which lays in the range of viral particle concentration found in sputum of infected individuals (Bar-On et al., 2020). The final Spike concentration in this solution was 18 μg/mL.

Expression and purification of human anti-Spike monoclonal antibodies

Expi293F™ cells (Thermo Fisher) were transfected with plasmids carrying J08 and 02M04 antibody heavy and the light chains with a 1:2 ratio using ExpiFectamineTM293 Transfection Kit (Thermo Fisher Scientific) as recommended by the manufacturer. Three and six days after transfection, cell cultures were harvested and clarified by centrifugation (1,100 g for 10 min at RT). Supernatants were recovered and filtered with 0.45 μm filter to remove particulate material. Purification process was conducted at room temperature using the ÄKTA Go purification system (GE Healthcare Life Sciences) through a 1 ml HiTrap Protein G HP column (GE Healthcare Life Sciences) previously equilibrated with Loading Buffer (0.02 M NaH2PO4 pH 7). Each monoclonal antibody was eluted from the column in 1 ml fractions of Elution Buffer (0.1 M glycine-HCl, pH 2.7) and collected in vials pre-dispensed with 100 μl of Neutralization Buffer (Tris-HCl pH 9.0). Protein-containing fractions were pooled and dialyzed in PBS 1x Buffer pH 7.4 with a 1:200 ratio using Slide-A-Lyzer™ Dialysis Cassettes, 10K MWCO, 3 mL (Thermo Fisher Scientific) at 4°C overnight. The final antibody concentration was determined by measuring the absorbance at 562 nm using Pierce™ BCA Protein Assay Kit (Thermo Scientific). Purified antibodies were stored at -80°C prior to use.

Spike binding assays

To analyze the binding of Spike protein to CTLs, 0.15×10^6 freshly purified $CD8^+$ T cells (day 0) and CTLs (day 7) were pre-treated with Spike W as described in “CTL pre-treatments”. Cells were then labelled with anti-Spike human J08 mAb for 30 min on ice. After washing with cold PBS, samples were incubated for 30 min on ice with Alexa Fluor 488- anti-human (#A11013, ThermoFisher Scientific) secondary antibody and then analyzed by confocal microscopy. Alternatively, 0.15×10^6 CTLs (day 7) were incubated with MiniV or control liposomes as described in “CTL pre-treatments” and analyzed by confocal microscopy.

CTL differentiation

$CD8^+$ T cells (1×10^6/ml) were stimulated and expanded in RPMI-HEPES supplemented with 10% BCS, 1% MEM NEAA and 50 Units/mL recombinant human IL-2 (Myltenyi; #130-097-745) with Dynabeads™ Human T-activator CD3/CD28 (Gibco, #11132D) the same day of the purification (day 0, also referred as resting $CD8^+$ T cells). 48 h after activation (day 2) the beads were removed and the cells expanded in RPMI-HEPES supplemented with 10% BCS, 1% MEM NEAA and 50 Units/mL recombinant human IL-2

for further three days (day 5). Five days post-purification, cells were further expanded for two days and collected at the day 7.

CTL pre-treatments

To allow for Spike binding on the cell surface, $CD8^+$ T cells (0.5×10^6) were incubated for 30 min at 20°C in 50 µl RPMI-HEPES in the absence of BCS with 2.5 µg Spike Wuhan/BA.1/BA.2 or PBS vehicle control (concentration of Spike treatment chosen based on a dose-response analysis; see Figure S2B). Alternatively, CTLs were pre-treated under the same conditions with 1.2×10^9/ml MiniVs or control liposomes. Spike-W and the Omicron BA.1 variant were also incubated in combination with the respective neutralizing mAbs (J08 and 02M04, respectively) at a 1:3 protein:antibody ratio. Alternatively, $CD8^+$ T cells (0.5×10^6) were incubated for 30 min at 20°C in 50 µl RPMI-HEPES in the absence of BCS with 2 µg/ml anti-ACE2 antibody (R&D Systems, #AF933) (Hoffmann et al., 2020), or the ACE2 substrate/ligand Angiotensin II (Merck, #A9525; 1 µM), or the ACE2 product Ang (1-7) (Sigma, #A9202; 1 µM).

For cytotoxicity assays, cells were pre-treated in the same conditions in serum-free AIM V medium (Gibco, #12055-091) (calcein release assays) or RPMI 1640 (flow cytometry-based assays). None of the treatments affected cell viability at the concentrations and times chosen for the analyses, as assessed by Trypan blue (Sigma-Aldrich, T8154) exclusion (see legend to figures 3 and 5).

$CD8^+$ T cell transfections

Freshly purified $CD8^+$ T cells were transiently transfected with the ACE2-GFP construct or GFP vector control (DNA/cells ratio = 1 µg/10^6 cells) using the Human T cell Nucleofector Kit (Amaxa Biosystem, #VPA-1002) and the Amaxa Nucleofector II system (Lonza), Program V-024, Cells were conjugated with SAg-loaded Raji cells 24 h after transfection.

Conjugate formation, immunofluorescence microscopy and analysis

Conjugates between $CD8^+$ T cells and superantigens-pulsed Raji B cells were carried out as previously described (Cassioli et al., 2021b). Raji B cells (0.08×10^6), used as APCs, were loaded with 10 µg/ml Staphylococcal superantigens A (SEA; Toxin Technologies, #AT101), B (SEB; Toxin Technologies, #BT202) and E (SEE; Toxin Technologies, #ET404) for 2 h and labelled with 10 µM Cell Tracker Blue for the last 15 min of the incubation with the superantigens (+ SAgs). The mix of SAgs was used to cover a substantial proportion of the TCR Vβ repertoire. Conjugates of $CD8^+$ T cells with Raji B cells formed in the absence of SAgs were used as negative controls (SAgs). Raji B cells, pulsed or not with SAgs, were washed twice, mixed with $CD8^+$ T cells (0.12×10^6) pre-treated as described above and incubated for 15 min at 37°C. The same conditions were used for IS experiments on BALs and PBLs from acutely infected COVID-19 patients, using as positive controls PBLs from healthy donors. To analyze early TCR signaling events a shorter time of incubation (5 min) was included. Samples for immunofluorescence analysis were seeded onto poly-L-lysine (Merck, #P1274)-coated slides (ThermoFisher Scientific, #X2XER208B) and fixed and permeabilized for 10 min in methanol at -20°C (for CD3ζ and PTyr staining) or fixed for 15 min with 4% paraformaldehyde/PBS at room temperature (for PCNT, P-ZAP70 and GzmB

staining). Following fixation, samples were washed in PBS for 5 min. PFA-fixed cells were permeabilized with 0.1% Triton, 1% BSA PBS. Following permeabilization, samples were washed in PBS for 5 min. Cells were stained with primary antibodies ([1:30] CD3ζ; [1:50] P-ZAP70; [1:100] PTyr; [1:200] PCNT; [1:50] GzmB; see above catalogue #) overnight at 4°C. After washing with PBS, samples were incubated for 45 min at room temperature with Alexa Fluor 488- and 555-labeled secondary antibodies and mounted with 90% glycerol/ PBS.

Confocal microscopy was carried out on a Zeiss LSM700 (Carl Zeiss, Jena, Germany) microscope using a 63x/1.40 oil immersion objective. Images were acquired with pinholes opened to obtain 0.8 μm-tick sections. Detectors were set to detect an optimal signal below the saturation limits. Images were processed with Zen 2009 image software (Carl Zeiss, Jena, Germany). Immunofluorescence analyses were carried out on medial optical sections of $CD8^+$ T cell:APC conjugates using ImageJ (version 1.53a). Relative distances (μm) of the centrosome (marked by PCNT) from the center of the contact site with the APC, and of the lytic granules (marked by GzmB) from the centrosome, were measured using ImageJ (FigS2A). Scoring of conjugates for accumulation of CD3ζ or P-Tyr at the IS, or for centrosome (PCNT) juxtaposition to the IS membrane, was based on the presence of the respective staining solely at the T cell-APC contact site and was expressed as percentage of conjugates with synaptic staining *versus* the total number of conjugates analyzed. Recruitment index was calculated for each marker as the ratio of CD3ζ or p-Tyr fluorescence intensity at the synaptic area, which is manually defined at the T cell-APC contact site, compared to the remaining T-cell area, using ImageJ.

Z-stacks were acquired on a spinning disk confocal and super-resolution microscope (CSU-W1-SoRA Nikon), with 60× oil objectives (numerical aperture 1.49) using a Photometrics BSI (Nikon). 3D Deconvolution (Richardson-Lucy method, 10 iterations) was applied to high-resolution imaging to improve contrast of video 2 and 3. 3D reconstructions were obtained using Fiji (version 2.1.0).

Flow cytometry and immunoblot

For flow cytometric analysis of protein tyrosine phosphorylation conjugates were formed as described in the “Conjugate formation, immunofluorescence microscopy and analysis” section and incubated for at 37°C 1, 5, 15 and 30 min. Raji B cells were labelled 1.5 μM carboxyfluorescein diacetate succinimidyl ester (CFSE,ThermoFisher, #C34554) in PBS for 8 min at room temperature, then the staining reaction was stopped by adding BCS. CFSE-stained Raji B cells (0.1×10^6) were co-cultured with $CD8^+$ T cells (0.150×10^6), pre-treated as described in “CTL pre-treatments” section, for different time points. Conjugates were fixed for 15 min with 4% paraformaldehyde/PBS, then permeabilized with BD Perm/ Wash™ Buffer (BD Biosciences, #51-2091KZ), stained with anti-PTyr antibodies (clone 4G10, #05-32, Merk Millipore) and processed for flow cytometry, gating on CFSE negative ($CFSE^-$) cells.

1×10^6 purified $CD8^+$ T cells (day 0) and CTLs (day 7) were used for immunoblot analysis of ACE2. For immunoblot analysis of Erk activation triggered by TCR cross-linking, CTLs (0.5×10^6 in 50 μl), pre-treated with Spike W or PBS as described in the section “CTL

pre-treatments", were activated for 0, 5 and 10 min at 37°C using anti-CD3ε (1 μg/ml, OKT3, #317302, Biolegend) and anti-CD28 (1 μg/ml, CD28.2, #302902, Biolegend) mAbs. Cells were pelleted, washed twice in ice-cold PBS and lysed in 10-15 μl lysis buffer (0.5% Triton X-100 in 20 mM Tris-HCl, pH 8.0, 150 mM NaCl) in the presence of protease inhibitors (Calbiochem, 539,134) and the phosphatase inhibitor sodium vanadate (Sigma-Aldrich, S6508). Lysates were cleared by centrifugation at 16,000xg for 20 min. Protein quantification in post-nuclear supernatants was carried out using the BCA Assay kit (EuroClone, EMP014500). Proteins were resolved by SDS-PAGE and transferred to nitrocellulose membranes (#10600002, Amersham Protran). Immunoblotting was carried out using anti-phospho-Erk1/2 ([1:500], phosphorylated p44/42 (MAPK) Erk1/2, #9101, Cell Signaling), anti-Erk2 ([1:500], clone D2, #sc-1647, SantaCruz), anti-ACE2 ([1:500], clone SN0754, #MA5-32307, Invitrogen) and anti-actin ([1:10000], #MAB1501, Merck Millipore) antibodies and peroxidase-labeled secondary Ig, and a chemiluminescence detection kit (Pierce Rockford). Stripping was carried out by using Re-Blot Plus Mild Antibody Stripping Solution, 10x (#2502, Merck Millipore). Blots were scanned using a laser densitometer (Duoscan T2500; Agfa, Milan, Italy) and quantified using ImageJ 1.53a (National Institutes of Health, USA).

RNA purification and RT-PCR

RNA was extracted from CTLs (days 0, 5 and 7) using the RNeasy Plus Mini Kit (Qiagen. #74136), reverse transcribed to first-strand cDNAs using iScript™ cDNA Synthesis Kit (Bio-Rad, #1708891) and analyzed by Real-time quantitative PCR (RT-qPCR) as previously described (Onnis et al., 2015). Primer sequences for ACE2 amplified a region of 133 bp (Forward: TCCATTGGTCTTCTGTCACCCGC; Reverse: AGACCATCCACCTCCACTTCTC). Primer sequences for MAS1 amplified a region of 121 bp (Forward: GCCCTGAGGAGACCGTAG; Reverse: ACAACAGCGGTTCTTGCTC. Primer sequences for GrzmB amplified a region of 121 bp (Forward: TCAAAGAACAGGAGCCGACC; Reverse: TTGGCCTTTCTCTCCAGCTG). Primer sequences for 18S amplified a region of 64 bp: Forward: CGCCGCTAGAGGTGAAATT; Reverse: CTTGGCAAATGCTTTCGC. Differences in gene expression were calculated using the ΔΔCt method and normalized to 18S.

Degranulation and cytotoxicity assays

For the degranulation assay, Raji B cells were incubated with 1.5 μM carboxyfluorescein diacetate succinimidyl ester (CFSE,ThermoFisher, #C34554) in PBS for 8 min at room temperature, then the staining reaction was stop by adding BCS. CFSE-stained Raji B cells (0.025×10^6) were loaded with 1 μg/ml Staphylococcal superantigens A, B and E (+SAgs) for 1 h in serum-free AIM V medium, then mixed with $CD8^+$ T cells (0.0625×10^6), pre-treated as described above, at an Effector:Target (E:T) ratio 2.5:1 in 50 μl AIMV medium containing APC-labelled anti-human CD107a (LAMP1) mAb (1:160) for 1 h at 37°C. Unpulsed CFSE-stained Raji B cells were used as negative control (-SAgs). Cells were washed, resuspended in cold PBS and acquired using a GUAVA flow cytometer (Merck Millipore). For immunofluorescence staining of surface LAMP1, cells were seeded onto poly-L-lysine-coated slides and fixed for 15 min in 4% paraformaldehyde/PBS at room temperature. Following fixation, samples were washed in PBS for 5 min. Cells were

incubated for 45 min at room temperature with Alexa Fluor 555-labeled secondary antibody and mounted with 90% glycerol/PBS.

For the cytotoxicity assay, Raji B cells were stained with 500 nM of calcein-AM (Invitrogen, #C1430) in serum-free AIM V medium with 10 mM HEPES for 15 min at room temperature, then loaded with 2 μg/ml Staphylococcal superantigens A, B and E (+SAgs) for 2 h in serum-free AIM V medium (Gibco, #12055-091). SAg-pulsed Raji B cells used as target cells were settled in a 96-well black flat bottom plate (5×10^4 cells per well). Unpulsed CFSE-stained Raji B cells were used as negative control (-SAgs). CTLs (day 7) were added to target cells at different E:T ratios (i.e. 5:1, 10:1, 20:1 for analysis of cytotoxicity of CTLs (day 7) (Fig.S1C) and 2.5:1, 5:1, 10:1 for analysis of cytotoxicity of CTLs (day 7) pre-treated with 0.05 μg/μl Spike W) (Fig.3F) in 200 μl AIMV medium and incubated at 37°C up to 4 h to measure killing. Target cells alone and target cells lysed with 1% Triton X-100 were used as control samples. The decreased calcein fluorescence in target cells due to cell lysis was measured at 485 nm excitation wavelength and 528 nm emission wavelength in the bottom reading mode by using a Synergy HTX multi-mode plate reader (BioTek). Cytotoxicity (% target cell lysis) was calculated as follows: $(F_{live} - \gamma \times F_{exp})/(F_{live} - F_{lyse}) \times 100$, where F_{live} is the fluorescence of only target cell controls, F_{exp} are the CTLs with target cells, and F_{lyse} is the maximal target lysis in the presence of 1% Triton X-100. The γ value was measured at time zero: $\gamma = F_{live}(0)/F_{exp}(0)$.

To analyse the effects of CTL pre-treatments on cytotoxicity using a flow cytometry-based and antigen-specific assay, melanoma-specific CTLs, pre-treated for 30 minutes at 20°C with either Spike-W (1, 2.5, 5 μg/ml), or 1.2×10^9/ml MiniVs, or 2 μg/ml anti-ACE2 Ab, or PBS, were co-cultured with melanoma A375 cells in RPMI 10% FCS. The experiment was performed in duplicate at an effector to target ratio of 5, 2.5 and 1. After 18 h, cells were collected and stained with FITC-labelled anti-CD8 mAb. Propidium iodide (Sigma, #537059) was added before of each acquisition to measure the frequency of dead A375 cells. Flow cytometric analysis was carried out on BD FACS Canto II using the FACSDiva software (Becton Dickinson, Franklin Lakes, NJ, USA).

ELISA

To measure IFNγ production, 2×10^5 CTLs specific for MAGE A3 melanoma antigen were seeded in duplicate in RPMI-1640 medium and co-cultured with 10^5 irradiated autologous antigen presenting cells and MAGE A3 antigen (2 μg/ml). CTLs of each melanoma patient were pre-treated with PBS or Spike (1, 2.5, 5 μg/ml) or anti-ACE2 Ab for 30 min at 20°C. Alternatively, CTLs were co-cultured with Spike-overexpressing A375 cells. Supernatant from each sample was collected after incubation for 36 h and then tested in duplicate for its content of IFNγ by ELISA (Invitrogen).

Statistics and reproducibility

Each experiment was performed at least 3 independent times. The exact number of repeats and the number of cells analyzed is specified in the figure legends. Statistical analyses were performed with Prism software (GraphPad Software). Pairwise or multiple comparisons of values with normal distribution were carried out with Student's *t*-test (paired or unpaired),

one-sample *t*-test (theoretical mean = 1) and One-way ANOVA test or One-sample *t*-test (theoretical mean =100), whereas values without Gaussian distribution were analysed with Mann-Whitney test or Kruskal-Wallis test. Statistical significance was defined as: ****$p \leq 0.0001$; *** $p \leq 0.001$; **$p \leq 0.01$; *$p \leq 0.05$; n.s., not significant.

Supplementary Material

Refer to Web version on PubMed Central for supplementary material.

Acknowledgements

The authors wish to thank Hsin-Fang Chang (University of Saarland, Germany) for sharing the calcein release protocol, Mike Dustin (University of Oxford, UK) for his support on the experiments with MiniVs and Jason S. McLellan (University of Texas, Austin, USA) for generously providing the SARS-CoV-2 S-2P encoding construct. This work was funded by ERC Synergy grant 951329 (ATTACK) and AIRC grant IG-2017-20148 to CTB, and ERC Advanced grant 787552 to RR (vAMRes). OS was funded by an ERC Marie Sklodowska Curie Actions/UK Engineering and Physical Science Research Council fellowship (EP/X023907/1). This work was supported by a fundraising activity promoted by Unicoop Firenze, Coop Alleanza 3.0, Unicoop Tirreno, Coop Centro Italia, Coop Reno e Coop Amiatina. The graphical abstract was created using BioRender.com.

List of non-standard abbreviations

ACE2	angiotensin-converting enzyme
Ang	angiotensin
COVID-19	coronavirus disease 2019
CFSE	carboxyfluorescein succinimidyl ester
GzmB	Granzyme B
IS	immune synapse
LG	lytic granule
MEM NEAA	MEM non-essential aminocids
MiniV	Minimal Virion
PCNT	pericentrin
RAS	renin-angiotensin system
SEA, SEB, SEE	Enterococcal Superantigen A, B, E
SAgs	Superantigens
Spike-W	Wuhan Spike

References

Amedei A, Della Bella C, Niccolai E, Stanflin N, Benagiano M, Duranti R, Del Prete G, Murphy TF, D'Elios MM. Moraxella catarrhalis-specific Th1 cells in BAL fluids of chronic obstructive

Europe PMC Funders Author Manuscripts

pulmonary disease patients. Int J Immunopathol Pharmacol. 2009; 22: 979–90. [PubMed: 20074461]

Andreano E, Nicastri E, Paciello I, Pileri P, Manganaro N, Piccini G, Manenti A, Pantano E, Kabanova A, Troisi M, Vacca F, et al. Extremely potent human monoclonal antibodies from COVID-19 convalescent patients. Cell. 2021a; 184: 1821–1835. e1816 [PubMed: 33667349]

Andreano E, Paciello I, Piccini G, Manganaro N, Pileri P, Hyseni I, Leonardi M, Pantano E, Abbiento V, Benincasa L, Giglioli G, et al. Hybrid immunity improves B cells and antibodies against SARS-CoV-2 variants. Nature. 2021b; 600: 530–535. [PubMed: 34670266]

Au-Yeung BB, Shah NH, Shen L, Weiss A. ZAP-70 in Signaling, Biology, and Disease. Annu Rev Immunol. 2018; 36: 127–156. [PubMed: 29237129]

Bastard P, Rosen LB, Zhang Q, Michailidis E, Hoffmann HH, Zhang Y, Dorgham K, Philippot Q, Rosain J, Beziat V, Manry J, et al. Autoantibodies against type I IFNs in patients with life-threatening COVID-19. Science. 2020; 370 eabd4585 [PubMed: 32972996]

Bar-On YM, Flamholz A, Phillips R, Milo R. SARS-CoV-2 (COVID-19) by the numbers. Elife. 2020; 9 e57309 [PubMed: 32228860]

Batista FD, Iber D, Neuberger MS. B cells acquire antigen from target cells after synapse formation. Nature. 2001; 411: 489–494. [PubMed: 11373683]

Blumenthal D, Burkhardt JK. Multiple actin networks coordinate mechanotransduction at the immunological synapse. J Cell Biol. 2020; 219

Camargo SM, Singer D, Makrides V, Huggel K, Pos KM, Wagner CA, Kuba K, Danilczyk U, Skovby F, Kleta R, Penninger JM, et al. Tissue-specific amino acid transporter partners ACE2 and collectrin differentially interact with hartnup mutations. Gastroenterology. 2009; 136: 872–882. [PubMed: 19185582]

Cassioli C, Baldari CT. The Expanding Arsenal of Cytotoxic T Cells. Front Immunol. 2022; 13 883010 [PubMed: 35514977]

Cassioli C, Balint S, Compeer EB, Felce JH, Gamberucci A, Della Bella C, Felce SL, Brunetti J, Valvo S, Pende D, D'Elios MM, et al. Increasing LFA-1 Expression Enhances Immune Synapse Architecture and T Cell Receptor Signaling in Jurkat E6.1 Cells. Front Cell Dev Biol. 2021a; 9 673446 [PubMed: 34368126]

Cassioli C, Onnis A, Finetti F, Capitani N, Brunetti J, Compeer EB, Niederlova V, Stepanek O, Dustin ML, Baldari CT. The Bardet-Biedl syndrome complex component BBS1 controls T cell polarity during immune synapse assembly. J Cell Sci. 2021b; 134 jcs258462 [PubMed: 34423835]

Chaouat AE, Brizic I, Kucan Brlic P, Atari N, Kliker L, Alfi O, Mandelboim M, Wolf D, Tafish L, Kol I, Jonjic S, et al. Anti-human ACE2 antibody neutralizes and inhibits virus production of SARS-CoV-2 variants of concern. iScience. 2022; 25 104935 [PubMed: 35992307]

Chemin K, Bohineust A, Dogniaux S, Tourret M, Guegan S, Miro F, Hivroz C. Cytokine secretion by CD4+ T cells at the immunological synapse requires Cdc42-dependent local actin remodeling but not microtubule organizing center polarity. J Immunol. 2012; 189: 2159–2168. [PubMed: 22821962]

Chen Y, Zhang YN, Yan R, Wang G, Zhang Y, Zhang ZR, Li Y, Ou J, Chu W, Liang Z, Wang Y, et al. ACE2-targeting monoclonal antibody as potent and broad-spectrum coronavirus blocker. Sig Transduct Target Ther. 2021; 6: 315.

Chen Z, John Wherry E. T cell responses in patients with COVID-19. Nat Rev Immunol. 2020; 20: 529–536. [PubMed: 32728222]

Chua RL, Lukassen S, Trump S, Hennig BP, Wendisch D, Pott F, Debnath O, Thurmann L, Kurth F, Volker MT, Kazmierski J, et al. COVID-19 severity correlates with airway epithelium-immune cell interactions identified by single-cell analysis. Nat Biotechnol. 2020; 38: 970–979. [PubMed: 32591762]

Clarke NE, Fisher MJ, Porter KE, Lambert DW, Turner AJ. Angiotensin converting enzyme (ACE) and ACE2 bind integrins and ACE2 regulates integrin signalling. PLoS One. 2012; 7 e34747 [PubMed: 22523556]

Coppo M, Bandinelli M, Berni A, Galastri S, Abbate R, Poggesi L, Marra F, Gensini GF, Boddi M. Ang II Upregulation of the T-lymphocyte renin-angiotensin system is amplified by low-grade inflammation in human hypertension. Am J Hypertens. 2011; 24: 716–723. [PubMed: 21394089]

D'Elios MM, Josien R, Manghetti M, Amedei A, de Carli M, Cuturi MC, Blancho G, Buzelin F, del Prete G, Soulillou JP. Predominant Th1 cell infiltration in acute rejection episodes of human kidney grafts. Kidney Int. 1997; 51: 1876–84. [PubMed: 9186878]

Daniele T, Hackmann Y, Ritter AT, Wenham M, Booth S, Bossi G, Schintler M, Auer-Grumbach M, Griffiths GM. A role for Rab7 in the movement of secretory granules in cytotoxic T lymphocytes. Traffic. 2011; 12: 902–911. [PubMed: 21438969]

Danilczyk U, Sarao R, Remy C, Benabbas C, Stange G, Richter A, Arya S, Pospisilik JA, Singer D, Camargo SM, Makrides V, et al. Essential role for collectrin in renal amino acid transport. Nature. 2006; 444: 1088–1091. [PubMed: 17167413]

Douanne T, Griffiths GM. Cytoskeletal control of the secretory immune synapse. Curr Opin Cell Biol. 2021; 71: 87–94. [PubMed: 33711784]

Dustin ML, Choudhuri K. Signaling and Polarized Communication Across the T Cell Immunological Synapse. Annu Rev Cell Dev Biol. 2016; 32: 303–325. [PubMed: 27501450]

Fackler OT, Alcover A, Schwartz O. Modulation of the immunological synapse: a key to HIV-1 pathogenesis? Nat Rev Immunol. 2007; 7: 310–317. [PubMed: 17380160]

Hoffmann M, Kleine-Weber H, Schroeder S, Kruger N, Herrler T, Erichsen S, Schiergens TS, Herrler G, Wu NH, Nitsche A, Muller MA, et al. SARS-CoV-2 Cell Entry Depends on ACE2 and TMPRSS2 and Is Blocked by a Clinically Proven Protease Inhibitor. Cell. 2020; 181: 271–280. e278 [PubMed: 32142651]

Inoue Y, Tanaka N, Tanaka Y, Inoue S, Morita K, Zhuang M, Hattori T, Sugamura K. Clathrin-dependent entry of severe acute respiratory syndrome coronavirus into target cells expressing ACE2 with the cytoplasmic tail deleted. J Virol. 2007; 81: 8722–8729. [PubMed: 17522231]

Irvine DJ, Purbhoo MA, Krogsgaard M, Davis MM. Direct observation of ligand recognition by T cells. Nature. 2002; 419: 845–849. [PubMed: 12397360]

Kabanova A, Sanseviero F, Candi V, Gamberucci A, Gozzetti A, Campoccia G, Bocchia M, Baldari CT. Human Cytotoxic T Lymphocytes Form Dysfunctional Immune Synapses with B Cells Characterized by Non-Polarized Lytic Granule Release. Cell Rep. 2016; 15: 9–18. [PubMed: 27052167]

Kalfaoglu B, Almeida-Santos J, Tye CA, Satou Y, Ono M. T-cell dysregulation in COVID-19. Biochem Biophys Res Commun. 2021; 538: 204–210. [PubMed: 33220925]

Kowalczuk S, Broer A, Tietze N, Vanslambrouck JM, Rasko JE, Broer S. A protein complex in the brush-border membrane explains a Hartnup disorder allele. FASEB J. 2008; 22: 2880–2887. [PubMed: 18424768]

Kummerow C, Schwarz EC, Bufe B, Zufall F, Hoth M, Qu B. A simple, economic, time-resolved killing assay. Eur J Immunol. 2014; 44: 1870–1872. [PubMed: 24599783]

Lambert DW, Clarke NE, Hooper NM, Turner AJ. Calmodulin interacts with angiotensin-converting enzyme-2 (ACE2) and inhibits shedding of its ectodomain. FEBS Lett. 2008; 582: 385–390. [PubMed: 18070603]

Liao M, Liu Y, Yuan J, Wen Y, Xu G, Zhao J, Cheng L, Li J, Wang X, Wang F, Liu L, et al. Single-cell landscape of bronchoalveolar immune cells in patients with COVID-19. Nat Med. 2020; 26: 842–844. [PubMed: 32398875]

Lin Q, Keller RS, Weaver B, Zisman LS. Interaction of ACE2 and integrin beta1 in failing human heart. Biochim Biophys Acta. 2004; 1689: 175–178. [PubMed: 15276642]

Martin-Cofreces NB, Sanchez-Madrid F. Sailing to and Docking at the Immune Synapse: Role of Tubulin Dynamics and Molecular Motors. Front Immunol. 2018; 9 1174 [PubMed: 29910809]

Mentlik AN, Sanborn KB, Holzbaur EL, Orange JS. Rapid lytic granule convergence to the MTOC in natural killer cells is dependent on dynein but not cytolytic commitment. Mol Biol Cell. 2010; 21: 2241–2256. [PubMed: 20444980]

Norris EG, Pan XS, Hocking DC. Receptor binding domain of SARS-CoV-2 is a functional alphav-integrin agonist. bioRxiv. 2022.

Onnis A, Finetti F, Patrussi L, Gottardo M, Cassioli C, Spano S, Baldari CT. The small GTPase Rab29 is a common regulator of immune synapse assembly and ciliogenesis. Cell Death Differ. 2015; 22: 1687–1699. [PubMed: 26021297]

Papa I, Vinuesa CG. Synaptic Interactions in Germinal Centers. Front Immunol. 2018; 9 1858 [PubMed: 30150988]

Park EJ, Myint PK, Appiah MG, Darkwah S, Caidengbate S, Ito A, Matsuo E, Kawamoto E, Gaowa A, Shimaoka M. The Spike Glycoprotein of SARS-CoV-2 Binds to beta1 Integrins Expressed on the Surface of Lung Epithelial Cells. Viruses. 2021; 13

Samavati L, Uhal BD. ACE2, Much More Than Just a Receptor for SARS-COV-2. Front Cell Infect Microbiol. 2020; 10: 317. [PubMed: 32582574]

Sender R, Bar-On YM, Gleizer S, Bernshtein B, Flamholz A, Phillips R, Milo R. The total number and mass of SARS-CoV-2 virions. Proc Natl Acad Sci USA. 2021; 118 e2024815118 [PubMed: 34083352]

Sigrist CJ, de Castro E, Cerutti L, Cuche BA, Hulo N, Bridge A, Bougueleret L, Xenarios I. New and continuing developments at PROSITE. Nucleic Acids Res. 2013; 41: D344–347. [PubMed: 23161676]

Silva-Filho JL, Caruso-Neves C, Pinheiro AA. Angiotensin II type-1 receptor (AT1R) regulates expansion, differentiation, and functional capacity of antigen-specific CD8(+) T cells. Sci Rep. 2016; 6 35997 [PubMed: 27782175]

Silva-Filho JL, Caruso-Neves C, Pinheiro AA. Targeting Angiotensin II Type-1 Receptor (AT1R) Inhibits the Harmful Phenotype of Plasmodium-Specific CD8(+) T Cells during Blood-Stage Malaria. Front Cell Infect Microbiol. 2017; 7: 42. [PubMed: 28261571]

Simons P, Rinaldi DA, Bondu V, Kell AM, Bradfute S, Lidke DS, Buranda T. Integrin activation is an essential component of SARS-CoV-2 infection. Sci Rep. 2021; 11 20398 [PubMed: 34650161]

Springer TA, Dustin ML. Integrin inside-out signaling and the immunological synapse. Curr Opin Cell Biol. 2012; 24: 107–115. [PubMed: 22129583]

Staufer O, Gupta K, Hernandez Bücher JE, Kohler F, Sigl C, Singh G, Vasileiou K, Yagüe Relimpio A, Macher M, Fabritz S, Dietz H, et al. Synthetic virions reveal fatty acid-coupled adaptive immunogenicity of SARS-CoV-2 spike glycoprotein. Nat Commun. 2022; 13: 868. doi: 10.1038/s41467-022-28446-x [PubMed: 35165285]

Torres JL, Ozorowski G, Andreano E, Liu H, Copps J, Piccini G, Donnici L, Conti M, Planchais C, Planas D, Manganaro N, et al. Structural insights of a highly potent pan-neutralizing SARS-CoV-2 human monoclonal antibody. Proc Natl Acad Sci U S A. 2022; 119 e2120976119 [PubMed: 35549549]

Welch JL, Xiang J, Chang Q, Houtman JCD, Stapleton JT. T-Cell Expression of Angiotensin-Converting Enzyme 2 and Binding of Severe Acute Respiratory Coronavirus 2. J Infect Dis. 2022; 225: 810–819. [PubMed: 34918095]

Wen W, Su W, Tang H, Le W, Zhang X, Zheng Y, Liu X, Xie L, Li J, Ye J, Dong L, et al. Immune cell profiling of COVID-19 patients in the recovery stage by single-cell sequencing. Cell Discov. 2020; 6: 31. [PubMed: 32377375]

Wrapp D, Wang N, Corbett KS, Goldsmith JA, Hsieh CL, Abiona O, Graham BS, McLellan JS. Cryo-EM structure of the 2019-nCoV spike in the prefusion conformation. Science. 2020; 367: 1260–1263. [PubMed: 32075877]

Yin W, Xu Y, Xu P, Cao X, Wu C, Gu C, He X, Wang X, Huang S, Yuan Q, Wu K, et al. Structures of the Omicron spike trimer with ACE2 and an anti-Omicron antibody. Science. 2022; 375: 1048–1053. [PubMed: 35133176]

Zhang H, Wada J, Hida K, Tsuchiyama Y, Hiragushi K, Shikata K, Wang H, Lin S, Kanwar YS, Makino H. Collectrin, a collecting duct-specific transmembrane glycoprotein, is a novel homolog of ACE2 and is developmentally regulated in embryonic kidneys. J Biol Chem. 2001; 276: 17132–17139. [PubMed: 11278314]

Zhang JD, Patel MB, Song YS, Griffiths R, Burchette J, Ruiz P, Sparks MA, Yan M, Howell DN, Gomez JA, Spurney RF, et al. A novel role for type 1 angiotensin receptors on T lymphocytes to limit target organ damage in hypertension. Circ Res. 2012; 110: 1604–1617. [PubMed: 22534490]

Zhang Q, Bastard P, Liu Z, Le Pen J, Moncada-Velez M, Chen J, Ogishi M, Sabli IKD, Hodeib S, Korol C, Rosain J, et al. Inborn errors of type I IFN immunity in patients with life-threatening COVID-19. Science. 2020; 370

Zheng M, Gao Y, Wang G, Song G, Liu S, Sun D, Xu Y, Tian Z. Functional exhaustion of antiviral lymphocytes in COVID-19 patients. Cell Mol Immunol. 2020; 17: 533–535. [PubMed: 32203188]

Europe PMC Funders Author Manuscripts

Europe PMC Funders Author Manuscripts

Summary statement

We report a new mechanism of immune evasion by SARS-CoV-2 based on direct disabling CTLs to form immune synapses through Spike protein binding to ACE2. This mechanism could contribute to the failure of the immune system to control SARS-CoV-2 infection.

Europe PMC Funders Author Manuscripts

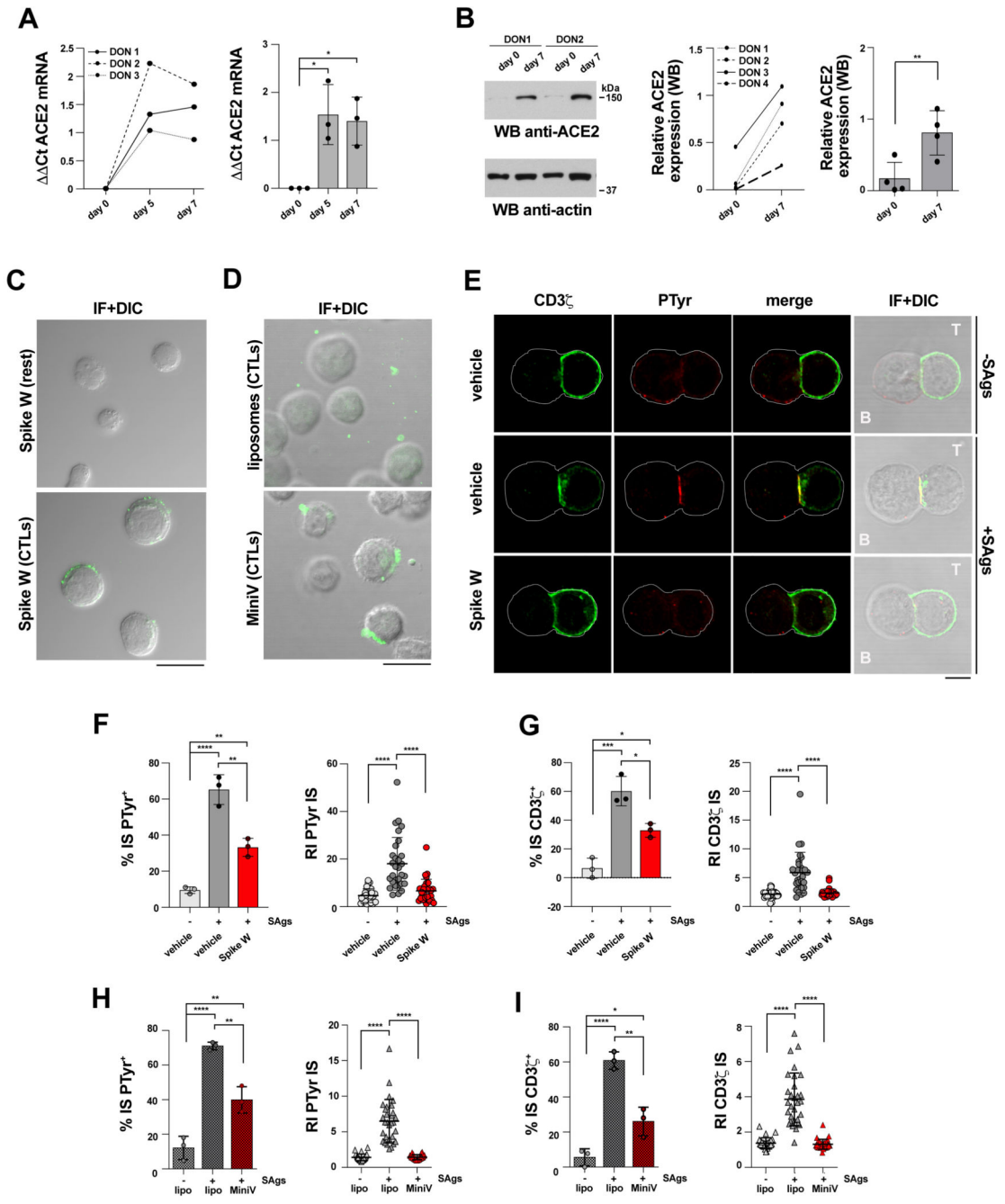

Figure 1. Spike suppresses TCR accumulation and phosphotyrosine signaling at the CTL IS.

A,B. Quantitative RT-PCR of human ACE2 mRNA (**A**) and immunoblot analysis of human ACE2 protein (**B**) in purified $CD8^+$ T cells prior to stimulation (day 0) or after stimulation with anti-CD3/CD28 mAb-coated beads in the presence of IL-2 for the indicated times. The migration of molecular mass markers is indicated. (n=3, One-way ANOVA test for qRT-PCR analysis, *$p \leq 0.05$; n=4, paired two-tailed Student's *t*-test for immunoblot analysis, **$p \leq 0.01$). **C**. Immunofluorescence analysis of Spike W binding to purified $CD8^+$ T cells prior to stimulation (day 0) or 7 days after stimulation with anti-CD3/CD28 mAb-coated

beads in the presence of IL-2 (n=2). Size bar, 15 μm. **D**. Immunofluorescence analysis of CTL binding of fluorescently labeled MiniVs (Spike W embedded in fluorescent NDP-labelled liposomes) or control liposomes. Representative images are shown (n=2). Size bar, 15 μm. **E-G**. Immunofluorescence analysis of CD3ζ and PTyr in CTLs (day 7) pre-treated with either vehicle (PBS) or 0.05μg/μl Spike Wuhan (Spike W; cell viability after pre-treatment 91.7±0.2%), mixed with Raji cells (APCs) either unpulsed or pulsed with a combination of SEA, SEB and SEE (SAgs), and incubated for 15 min at 37°C. Representative images (medial optical sections) of the T cell:APC conjugates are shown (**E**). Size bar, 5 μm. **F**. *Left*,Quantification (%) of 15-min SAg-specific conjugates harboring PTyr staining at the IS (≥50 cells/sample, n=3, One-way ANOVA test, ****$p \leq 0.0001$; **$p \leq 0.01$). *Right*,Relative PTyr fluorescence intensity at the IS (recruitment index) (10 cells/sample, n=3, Kruskal-Wallis test, ****$p \leq 0.0001$). **G**. *Left*, Quantification (%) of 15-min SAgspecific conjugates harboring CD3ζ staining at the IS (≥50 cells/sample, n=3, Oneway ANOVA test, *** $p \leq 0.001$; *$p \leq 0.05$). *Right*, Relative CD3ζ fluorescence intensity at the IS (recruitment index) (10 cells/sample, n=3, Kruskal-Wallis test, ****$p \leq 0.0001$). **H,I**. Immunofluorescence analysis of CD3ζ and PTyr in CTLs (day 7) pre-treated with either 1.2×10^9 control liposomes or MiniVs, mixed with Raji cells (APCs) either unpulsed or pulsed with a combination of SEA, SEB and SEE (SAgs), and incubated for 15 min at 37°C. **H**. *Left*, Quantification (%) of 15-min SAg-specific conjugates harboring PTyr staining at the IS (≥50 cells/sample, n=3, One-way ANOVA test, ****$p \leq 0.0001$; **$p \leq 0.01$). *Right*, Relative PTyr fluorescence intensity at the IS (recruitment index) (10 cells/sample, n=3, Kruskal-Wallis test, ****$p \leq 0.0001$). Side-by-side comparison of $PTyr^+$ immune synapses formed by CTLS pre-treated with the same amount of soluble and MiniV-associated Spike showed a ~2.3-fold increase in the suppressive ability of Spike when associated to MiniVs (51% vs 22%, n=3). **I**. *Left*,Quantification (%) of 15-min SAg-specific conjugates harboring CD3ζ staining at the IS (≥50 cells/sample, n=3, One-way ANOVA test, ****$p \leq 0.0001$; **$p \leq 0.01$; *$p \leq 0.05$.). *Right*, Relative CD3ζ fluorescence intensity at the IS (recruitment index) (10 cells/sample, n=3, Kruskal-Wallis test, ****$p \leq 0.0001$). Non-significant differences are not shown. Source data are available for this figure: SourceData F1

Europe PMC Funders Author Manuscripts

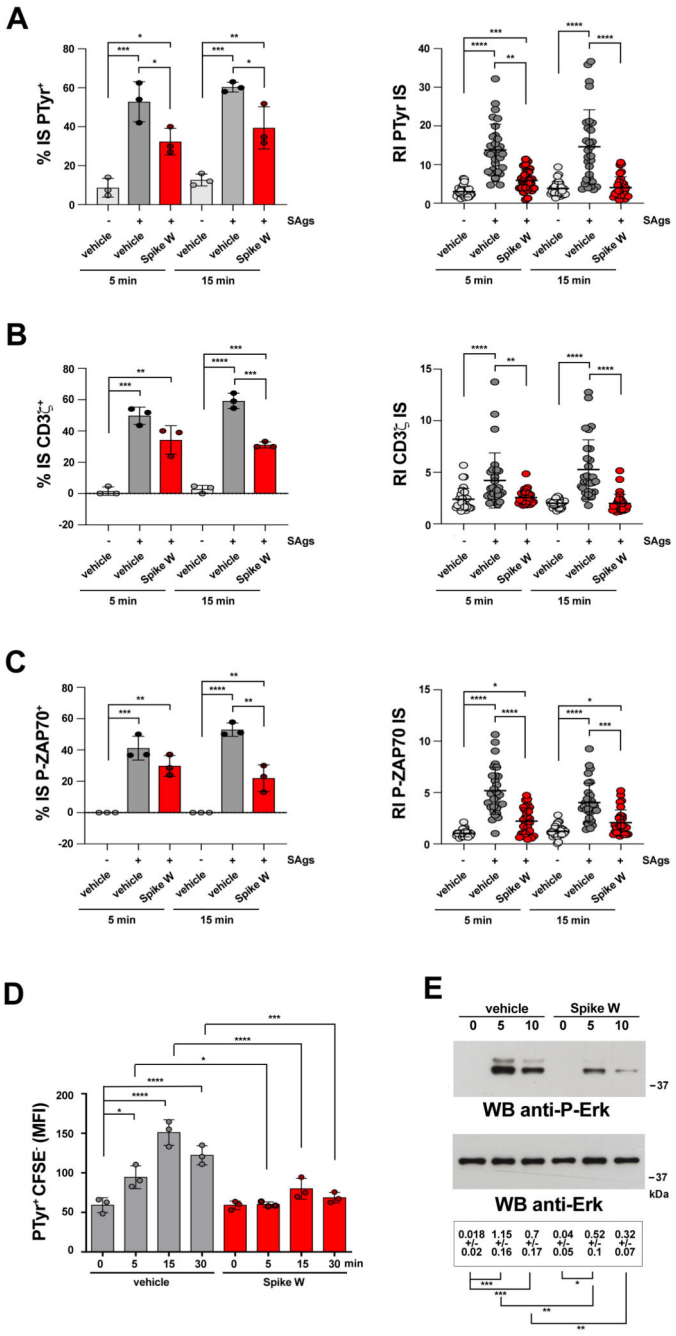

Figure 2. Spike suppresses signaling at an early step of IS assembly.

A-C. *Left*, Quantification (%) of 5-min and 15-min SAg-specific conjugates harboring PTyr (**A**), CD3ζ (**B**), or P-ZAP-70 (**C**) staining at the IS in CTLs (day 7) pre-treated with either vehicle (PBS) or 0.05μg/μl Spike Wuhan (Spike W), then mixed with Raji cells (APCs) either unpulsed or pulsed with a combination of SEA, SEB and SEE (SAgs), and incubated for 5 or 15 min at 37°C (≥50 cells/sample, n=3, One-way ANOVA test, ****$p \leq 0.0001$; *** $p \leq 0.001$; **$p \leq 0.01$; *$p \leq 0.05$). *Right*, Relative PTyr (**A**), CD3ζ (**B**), or P-ZAP-70 (**C**) fluorescence intensity at the IS (recruitment index) (10 cells/sample, n=3, Kruskal-Wallis

test, ****$p \leq 0.0001$; *** $p \leq 0.001$; **$p \leq 0.01$; *$p \leq 0.05$). **D**. Flow cytometric analysis of protein tyrosine phosphorylation in conjugates prepared as in (**A-C**) and incubated at 37°C for the indicated times. Raji cells were loaded with 1.5 μM CFSE prior to conjugate formation. Conjugates were stained with anti-PTyr mAb followed by fluorescently labelled secondary Abs. The analysis was carried out gating on $CSFE^-$cells (n=3, One-way ANOVA test, ****$p \leq 0.0001$; *** $p \leq 0.001$; *$p \leq 0.05$). **E**. Immunoblot analysis of Erk phosphorylation in CTLs activated with anti-CD3 and anti-CD28 mAbs. CTLs were incubated at 37°C for the indicated times and processed for immunoblot with antibodies against the active forms of Erk1/2. Stripped filters were blotted with anti-Erk2 mAb as loading control. The migration of molecular mass markers is indicated (n=2, One-way ANOVA test, *** $p \leq 0.001$; **$p \leq 0.01$; *$p \leq 0.05$). Data are expressed as mean±SD. ****$p \leq 0.0001$; *** $p \leq 0.001$; **$p \leq 0.01$; *$p \leq 0.05$. Non-significant differences are not shown. Source data are available for this figure: SourceData F1

Europe PMC Funders Author Manuscripts

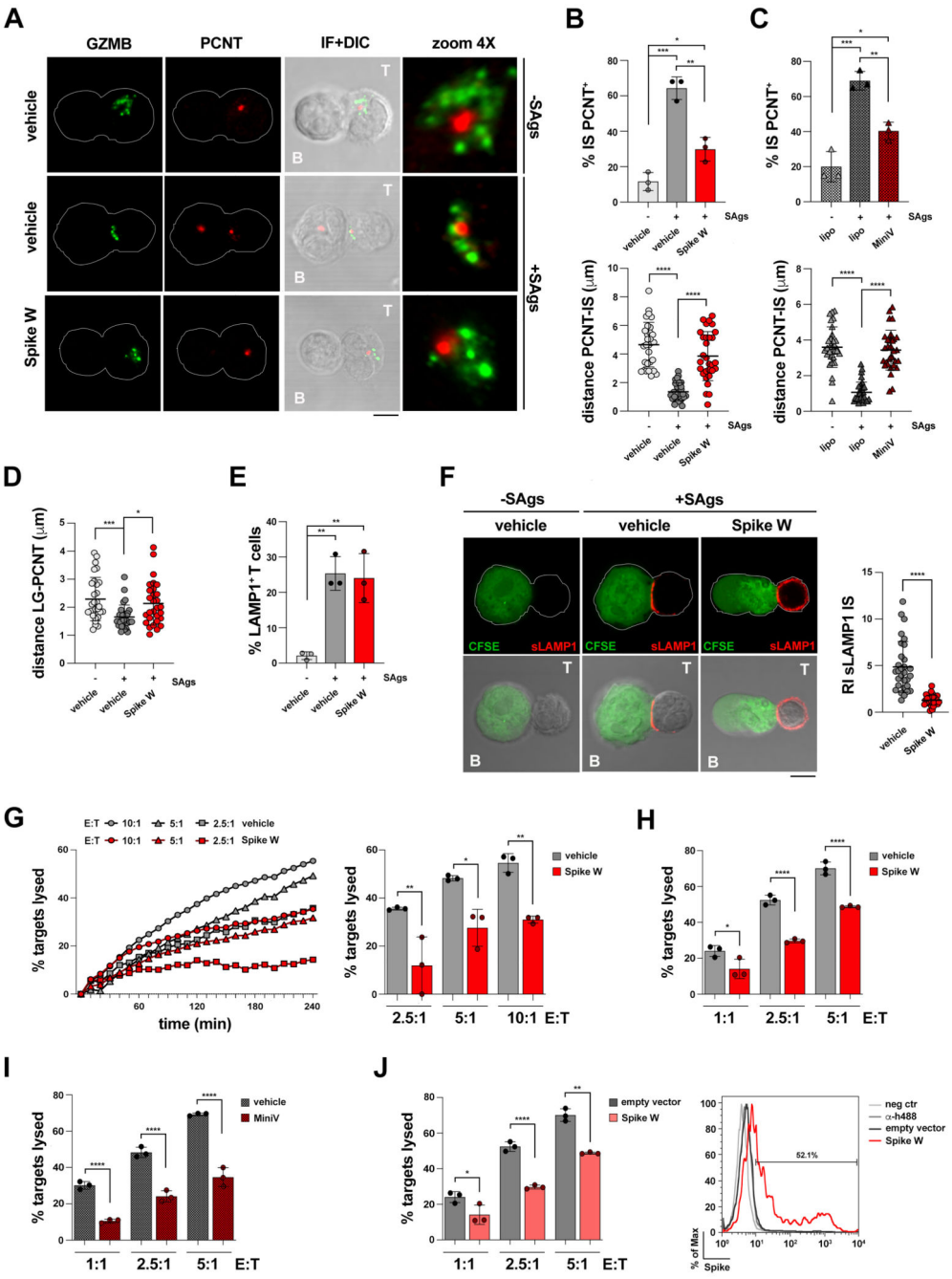

Figure 3. Spike inhibits centrosome and lytic granule polarisation to the CTL IS and CTL-mediated cytotoxicity.

A-D. Immunofluorescence analysis of PCNT and GrzmB in CTLs (day 7) pre-treated with either vehicle (PBS) or 0.05 μg/μl Spike Wuhan (Spike W) (**A,B,D**), or with 1.2×10^9 control liposomes or MiniVs (**A-C**), then mixed with Raji cells (APCs) either unpulsed or pulsed with a combination of SEA, SEB and SEE (SAgs), and incubated for 15 min at 37°C. Representative images (medial optical sections) of the conjugates are shown (**A**). **B,C**. *Top*, Quantification (%) of 15-min SAg-specific conjugates harboring PCNT

staining at the IS (≥50 cells/sample, n=3, One-way ANOVA test, *** $p \leq 0.001$; ** $p \leq 0.01$; * $p \leq 0.05$). *Bottom*, Measurement of the distance (μm) of the centrosome (PCNT) from the CTL-APC contact site (10 cells/sample, n=3, One-way ANOVA test, **** $p \leq 0.0001$). **D**. Measurement of the distance (μm) of the lytic granules (LG, marked by GzmB) from the centrosome (PCNT) in conjugates formed with Spike W-pre-treated CTLs (10 cells/sample, n=3, Kruskal-Wallis test, *** $p \leq 0.001$; * $p \leq 0.05$) (see figure S2 for parameters used for measurements plotted in panels B-D). **E**. Flow cytometry analysis of degranulation of CTLs (day 7) pre-treated with either vehicle (PBS) or Spike Wuhan (Spike W) and co-cultured with CFSE-stained Raji cells loaded with SAg at an E:T cell ratio 2.5:1 for 1 h. The histogram shows the percentage (%) of $LAMP1^+$ T cells (n=3, One-way ANOVA test, ** $p \leq 0.01$). **F**. Immunofluorescence analysis of degranulation of CTLs (day 7) pre-treated with either vehicle (PBS) or Spike Wuhan (Spike W) and co-cultured with CFSE-stained Raji cells loaded with SAg at an E:T cell ratio 2.5:1 for 1 h. Conjugates were fixed and stained without prior permeabilization with anti-LAMP1 mAb and fluorescently labelled secondary Abs to detect plasma membrane-associated LAMP1. The histogram shows the relative surface LAMP1 fluorescence (sLAMP1) intensity at the IS (recruitment index) of SAg-specific conjugates in the absence or presence of Spike (10 cells/sample, n=3, Kruskal-Wallis test, **** $p \leq 0.0001$). Negative control conjugates (no SAg) were not quantified as no sLAMP1 fluorescence was detectable. Representative images (medial optical sections) of the conjugates are shown. **G**. Fluorimetric analysis of cytotoxicity of CTLs (day 7) using the calcein release assay. CTLs were pre-treated with either vehicle (PBS) or Spike Wuhan (Spike W) and co-cultured with SAg-pulsed, calcein AM-loaded Raji cells at different E:T cell ratios for 4 h. The representative curves show the kinetics of target cell lysis by CTLs at the indicated E:T cell ratios. The histogram shows the target cell lysis at 4 h (n=3, One-way ANOVA test, ** $p \leq 0.01$; * $p \leq 0.05$). **H,I**. Flow cytometric analysis of antigen-specific target cell killing by melanoma-specific CTLs derived from 3 patients, pre-treated with either vehicle (PBS) or Spike Wuhan (Spike W), or with 1.2×10^9 control liposomes or MiniVs, using as target the melanoma cell line A375. Cells were co-cultured for 18 h and stained with propidium iodide and anti-CD8 mAb prior to processing for flow cytometry. Analyses were carried out gating on $CD8^-/PI^+$ cells. The histograms show the percentage (%) of target cells lysed (n=3, One-way ANOVA test, **** $p \leq 0.0001$; * $p \leq 0.05$). **J**. Flow cytometric analysis of antigen-specific target cell killing by melanoma-specific CTLs derived from 3 patients, using as target A375 melanoma cells transiently transfected with either a construct encoding Spike-W or the empty control vector (54.0±1.7 % transfected cells, as assessed by flow cytometric analysis with anti-Spike mAb J08; representative flow cytometric data are shown). Cells were co-cultured for 18 h and processed as in (**I**). The histograms show the percentage (%) of target cells lysed (n=3, One-way ANOVA test, **** $p \leq 0.0001$; ** $p \leq 0.01$; * $p \leq 0.05$). Data are expressed as mean±SD. Size bar, 5 μm.. Non-significant differences are not shown.

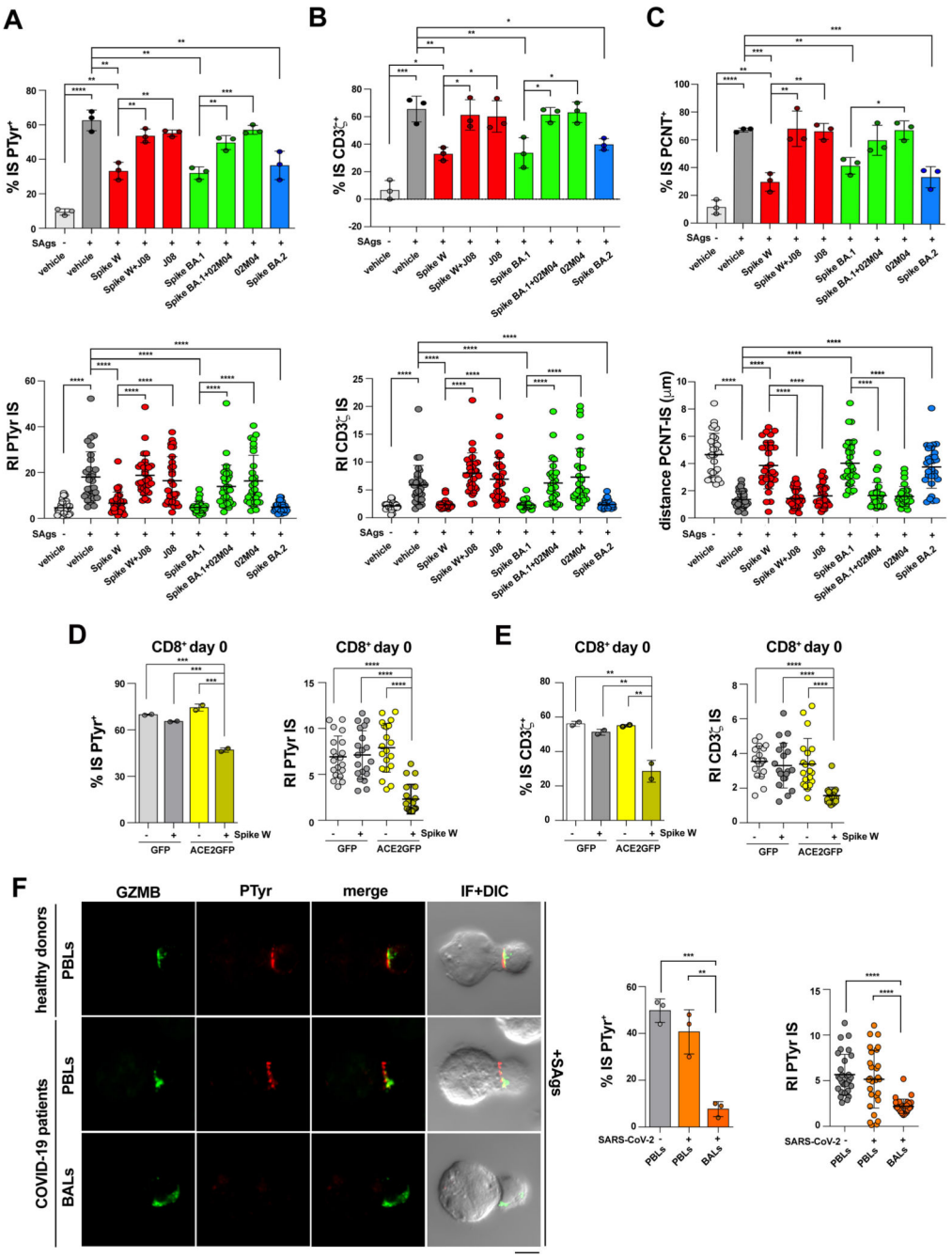

Figure 4. The inhibitory effects of Spike on IS formation are mediated by ACE2 and can be detected in acutely infected SARS-CoV-2 patients.

A,B. *Top*, Quantification (%) of 15-min antigen-specific conjugates harboring PTyr (**A**) or CD3ζ (**B**) staining at the IS in CTLs (day 7) pre-treated with either vehicle (PBS) or 0.05μg/μl Spike Wuhan (Spike W), Spike Omicron BA.1 (Spike BA.1), alone or in the presence of the respective neutralizing mAb (Spike W+J08; Spike BA.1+02M04); or Spike Omicron BA.2 (Spike BA.2). Samples pre-treated with only the neutralizing mAbs (J08 and 02M04) were also included in the analysis. CTLs were mixed with Raji cells

Europe PMC Funders Author Manuscripts

(APCs), either unpulsed or pulsed with a combination of SEA, SEB and SEE (SAgs), and incubated for 15 min at 37°C (≥50 cells/sample, n=3, unpaired two-tailed Student's *t*-test, ****$p \leq 0.0001$; *** $p \leq 0.001$; **$p \leq 0.01$; *$p \leq 0.05$). *Bottom*, Relative PTyr (**A**) or CD3ζ(**B**) fluorescence intensity at the IS (recruitment index) (10 cells/sample, n=3, Kruskal-Wallis test, ****$p \leq 0.0001$). **C**. *Top*, Quantification (%) of 15-min antigen-specific conjugates formed as in panel A harboring PCTN1 staining at the IS (≥50 cells/sample, n=3, One-way ANOVA test, ****$p \leq 0.0001$; *** $p \leq 0.001$; **$p \leq 0.01$; *$p \leq 0.05$). *Bottom*, Measurement of the distance (μm) of the centrosome (PCNT) from the T cell-APC contact site (10 cells/sample, n=3, Kruskal-Wallis test, ****$p \leq 0.0001$). **D,E**. Immunofluorescence analysis of PTyr (**D**) and CD3ζ (**E**) in purified $CD8^+$ T cells transfected with an ACE2-GFP-expressing construct or empty vector, pre-treated with either vehicle (PBS) or 0.05 μg/μl Spike Wuhan (Spike W), then mixed with Raji cells (APCs) either unpulsed or pulsed with a combination of SEA, SEB and SEE (SAgs), and incubated for 15 min at 37°C. The histograms show *(left)* the quantification (%) of conjugates harboring PTyr (**D**) and CD3ζ(**E**) staining at the IS (top) (≥50 cells/sample, n=2, One-way ANOVA test, *** $p \leq 0.001$; **$p \leq 0.01$), or *(right)* the relative PTyr (**D**) and CD3ζ (**E**) fluorescence intensity at the IS (recruitment index) (10 cells/sample, n=2, Kruskal-Wallis test, ****$p \leq 0.0001$). Quantification was carried out on GFP^+ cells. **F**. Immunofluorescence analysis of PTyr and GrzB in BALs or PBLs from patients with acute SARS-CoV-2 infection, or PBLs from healthy donors, mixed with Raji cells (APCs) pulsed with a combination of SEA, SEB and SEE (SAgs), and incubated for 15 min at 37°C. Representative images (medial optical sections) of the T cell:APC conjugates are shown. The histograms show (*left*) the quantification (%) of 15-min SAg-specific conjugates harboring PTyr staining at the IS (≥50 cells/sample, n=3, One-way ANOVA test, *** $p \leq 0.001$; **$p \leq 0.01$), or *(right)* the relative PTyr fluorescence intensity at the IS (recruitment index) (10 cells/sample, n=3, Kruskal-Wallis test, ****$p \leq 0.0001$). The analysis was restricted to CTLs, identified by GrzB staining. Data are expressed as mean±SD. Non-significant differences are not shown. Size bar, 5 μm.

Europe PMC Funders Author Manuscripts

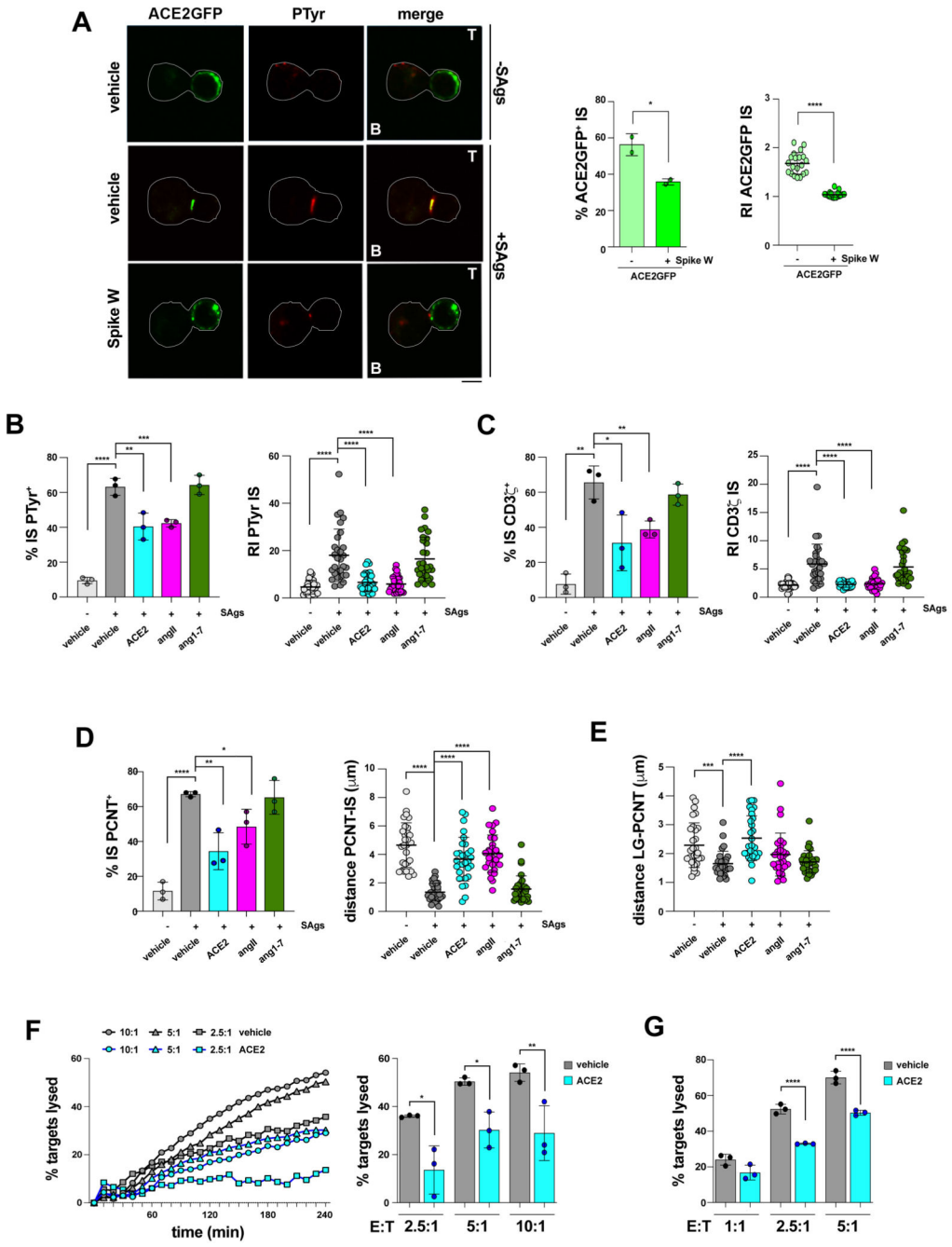

Figure 5. ACE2 is recruited to the CTL IS and suppresses IS formation and cytotoxicity.

A. Immunofluorescence analysis of ACE2 localization in purified $CD8^+$ T cells transfected with an ACE2-GFP-expressing construct or empty GFP vector, pre-treated with either vehicle (PBS) or 0.05 μg/μl Spike Wuhan (Spike W), then mixed with Raji cells (APCs) either unpulsed or pulsed with a combination of SEA, SEB and SEE (SAgs), and incubated for 15 min at 37°C. Representative images are shown. The histograms show *(left)* the quantification (%) of conjugates harboring ACE2-GFP staining at the IS (≥50 cells/sample, n=2, One-way ANOVA test, *$p \leq 0.05$), or *(right)* the relative ACE2-GFP

fluorescence intensity at the IS (recruitment index) (10 cells/sample, n=2, Kruskal-Wallis test, ****$p \leq 0.0001$). **B,C**. *Left*, Quantification (%) of 15-min conjugates harboring PTyr (**B**) or CD3ζ (**C**) staining at the IS. CTLs (day 7) were conjugated with Raji cells (APCs) in the absence or presence of SAgs and either an anti-ACE2 Ab (cell viability after pre-treatment 93.7±0.8%), or angiotensin II (AngII), or the peptide angiotensin 1-7 (Ang 1-7) (≥50 cells/sample, n=3, One-way ANOVA test, ****$p \leq 0.0001$; *** $p \leq 0.001$; **$p \leq 0.01$; *$p \leq 0.05$). *Right*, Relative PTyr (**B**) or CD3ζ (**C**) fluorescence intensity at the IS (recruitment index) (10 cells/sample, n=3, Kruskal-Wallis test, ****$p \leq 0.0001$). **D**. *Left*, Quantification (%) of 15-min conjugates formed as in panel A harboring PCTN staining at the IS (≥50 cells/sample, n=3, One-way ANOVA test, ****$p \leq 0.0001$; **$p \leq 0.01$; *$p \leq 0.05$). *Right*, Measurement of the distance (μm) of the centrosome (PCNT) from the T cell-APC contact site in CTL-APC conjugates formed as in panel A (10 cells/sample, n=3, Kruskal-Wallis test, ****$p \leq 0.0001$). **E**. Measurement of the distance (μm) of the lytic granules (LG, marked by GzmB) from the centrosome (PCNT) in 15-min CTL-APC conjugates formed as in panel A (10 cells/sample, n=3, Kruskal-Wallis test, ****$p \leq 0.0001$; *** $p \leq 0.001$). **F**. Fluorimetric analysis of cytotoxicity of CTLs (day 7) using the calcein release assay. CTLs were pre-treated with either vehicle (PBS) or 2 μg/ml anti-ACE2 Ab (ACE2) and co-cultured with SAg-pulsed, calcein AM-loaded Raji cells at different E:T cell ratios for 4 h. The representative curves show the kinetics of target cell lysis by CTLs at the indicated E:T cell ratios. The histogram shows the target cell lysis at 4 h (n=3, One-way ANOVA test, **$p \leq 0.01$; *$p \leq 0.05$). **G**. Flow cytometric analysis of antigen-specific target cell killing by melanoma-specific CTLs derived from 3 patients, using as target the melanoma cell line A375. CTLs were pre-treated as in panel **F**, co-cultured with A375 cells for 18 h and processed for flow cytometry after staining with propidium iodide and anti-CD8 mAb. Analyses were carried out gating on $CD8^-/PI^+$ cells. The histograms show the percentage (%) of target cells lysed (n=3, One-way ANOVA test, ****$p \leq 0.0001$). The data are expressed as mean±SD.. Non-significant differences are not shown. Size bar, 5 μm.